OPTIMIZATION OF ENHANCEMENTS TO ALUMINUM-BASED STRUCTURAL ENERGETIC MATERIALS

BY

NICHOLAS POIRIER

THESIS

Submitted in partial fulfillment of the requirements
for the degree of Master of Science in Mechanical Engineering
in the Graduate College of the
University of Illinois at Urbana-Champaign, 2018

Urbana, Illinois

Adviser:

Professor Nick Glumac

ABSTRACT

Warhead casings are most often made of steel due to its low cost, high strength, good manufacturability, and ability to produce dense high-speed fragments. However, inert steel does not improve blast wave characteristics. In fact, it significantly reduces peak blast pressure and impulse as energy is expended in fracturing the case and accelerating the fragments. In applications where fragmentation is unnecessary or unwanted, warhead energy output can be improved by choosing a case material that reacts in the detonation environment. Aluminum is a good candidate for this application due to its low cost, widespread availability, good manufacturability, and high enthalpy of combustion. Difficulty arises in the timely ignition of the aluminum. A plain aluminum case produces mostly large fragments which do not burn on the timescale necessary for primary blast enhancement. Alloying other elements as well as incorporating changes to case geometry can enhance breakup to improve early time ignition.

This research aims to optimize several parameters to maximize aluminum casing performance. Primary diagnostics consist of dynamic pressure measurements, quasi-static pressure measurements, and high speed imaging. Effect of wall material on fragment reaction is also investigated. Additionally, tensile test specimens are fabricated and tested to verify that structural properties of the aluminum are not compromised by the optimizations. Electron microscopy is used to examine case structure after the manufacturing, which was done here at the UIUC.

ACKNOWLEDGEMENTS

I would like to thank Professor Nick Glumac for offering his guidance during my time here as well as providing me the opportunity to work on several other related and unique projects. Additionally, I would like to thank Professor Emeritus Herman Krier for reviewing this thesis document.

I would also like to thank Professor Emeritus James Phillips for his assistance in using the Talbot material testing facilities and his insights in material science.

Finally, I would like to thank my fellow research group graduate students: David Amondson, Young Desanti, Rylie Lodes, Christopher Murzyn. Brian Read, Kevin Schafer, Joel Schwallier, and Emily Weerakkody. Their intelligence was always helpful and made both office and lab work enjoyable. I hope to maintain these friendships for years to come.

This research was supported by the Defense Threat Reduction Agency under contract HDTRA1-17-10006.

TABLE OF CONTENTS

CHAPTER 1: INTRODUCTION

1.1 Motivation

Long duration, high temperature fireballs are of interest in the defeat of biological weapons. Metal additives, such as aluminum, are commonly added to explosives to increase energy release, overpressures, and fireball temperatures. Aluminum powder has been a common additive to high explosive (HE) material. However, if either charge mass or volume are fixed then any added aluminum powder invariably replaces HE, lowering performance. The typically inert case material represents another possible source of energy in the detonation environment without reducing HE mass. Aluminum remains a promising candidate due to its good structural properties and potential for its energy release. Considering typical case mass to charge mass ratios and the high enthalpy of combustion of aluminum, even a fairly small amount of case combustion can significantly increase total system energy output.

Table 1.1: Energy release of selected materials

Material	Molar Mass(g/mol)	Detonation Enthalpy(kJ/g)	Combustion Enthalpy(kJ/g)
TNT	227.13	4.47	15.0
RDX	222.12	5.03	9.54
HMX	296.15	5.00	9.52
Aluminum	26.98	N/A	30.9
Magnesium	24.31	N/A	24.7

1.2 Casing Performance Metrics

The detonation of a high explosive converts condensed matter into hot gaseous products on the order of microseconds. The hot gaseous products rapidly expand to create a shockwave through the surrounding medium. The initial shockwave does much of the damage in an explosive event due to the sharp pressure rise as well as the total momentum imparted to a target. The pressure decays to below ambient before returning to ambient. The performance metrics of peak blast pressure and impulse are defined and shown in Figure 1.1 [1]. The peak blast pressure is simply the largest pressure observed in the initial blast, and the impulse is the integrated area under the pressure-time curve of the first positive phase of the blast. These metrics are typically much lower for cased explosives than bare explosives, due to energy being expended in fragmentation and to

the acceleration of the case material. Increases of peak blast pressure and impulse with a reactive case is an indication of prompt reactivity of the case material.

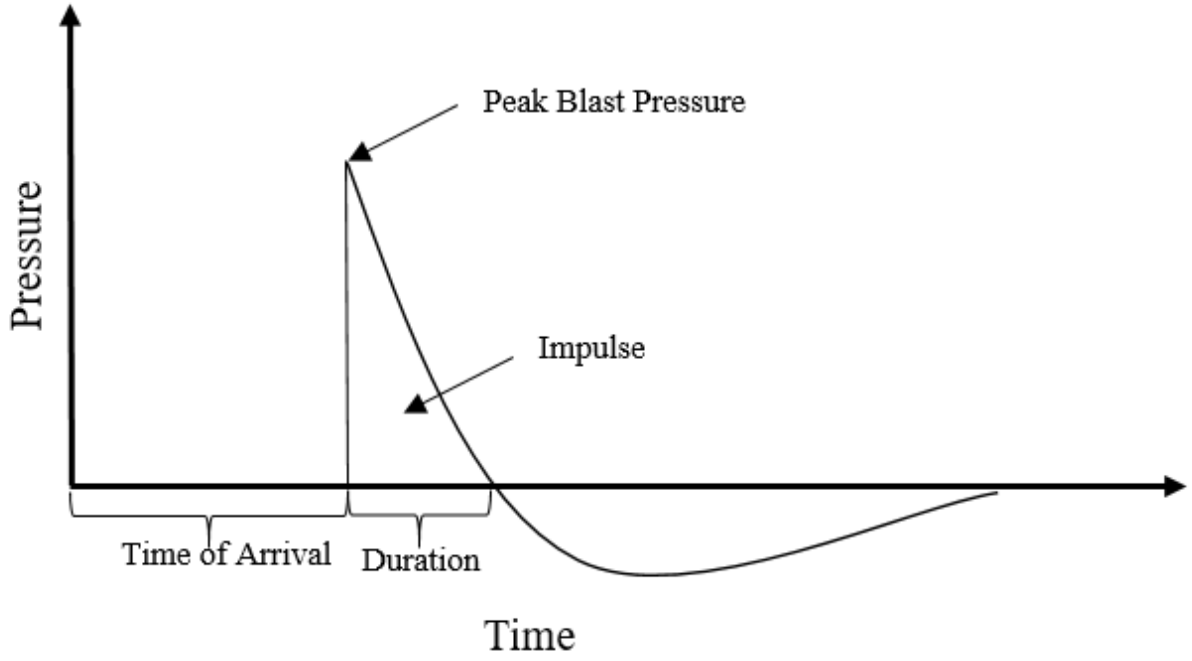

Figure 1.1: Initial blast wave phenomenon

Another important metric is the Quasi-Static Pressure (QSP). This is defined as the long-duration overpressure created in the sealed test chamber. The pressure rise can be directly attributed to a temperature rise the chamber air caused by the high explosive reaction and ensuing reflected shockwaves doing work on the air. This is shown in Figure 1.2. The chamber air can be assumed to be an ideal gas of known composition and volume. If heat loss to the chamber walls are neglected, then QSP can be directly related to the energy released in the test. A partially vented chamber can be accounted for with an exponential fit if needed to calculate the QSP at the time of detonation. It is important to note that QSP does not differentiate when the energy was released. It will be shown in a later section that secondary reaction of fragments impacting the chamber walls can also release a significant amount of energy and increase the QSP measurement. This energy release does not contribute to the initial blast and would not be present in a free field scenario [2].

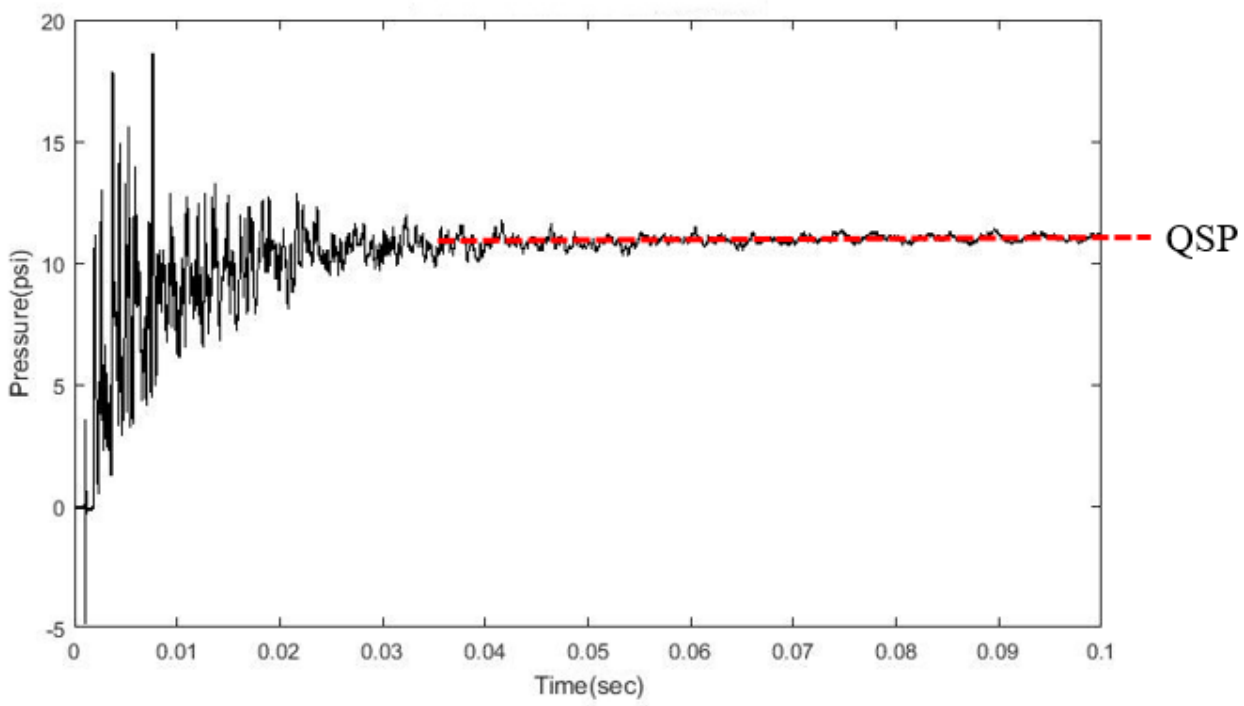

Figure 1.2: QSP fit to example data

1.3 Previous Work

A study performed by M. Clemenson at the University of Illinois Urbana-Champaign experimentally investigated a variety of variations to a pure aluminum case to enhance aluminum reactivity at the 10g scale [3]. Geometric variations such as axial holes, surface textures, and inserts were tested. Additionally, alloy variations were tested such as Al 5083, lithium, gallium, and magnesium. The motivation behind those modifications was to bias fragmentation towards smaller fragments, to reduce ignition temperature of the material, or to induce turbulent mixing of the detonation products with the ambient atmosphere. Other factors such as end confinement, atmospheric composition, and chamber wall material were also investigated. It was found that the best performing geometric variation was the inclusion of tungsten mesh in a cast aluminum case. The best performing alloy variations were the cast aluminum cases with a small percentage of added magnesium or lithium. It was observed that geometric variations primarily enhanced blast and impulse measurements while alloy variations primarily showed improved overall energy release through late combustion and impact induced reaction of fragments at the chamber walls. Additionally, it was found that end confinement of the casings significantly affected pressure dynamics as escaping hot detonation products reduce case fragmentation and the combustion. A

schematic of the setup used by Clemenson is shown in Figure 1.3 and several experimental cases are shown in Figure 1.4 [3].

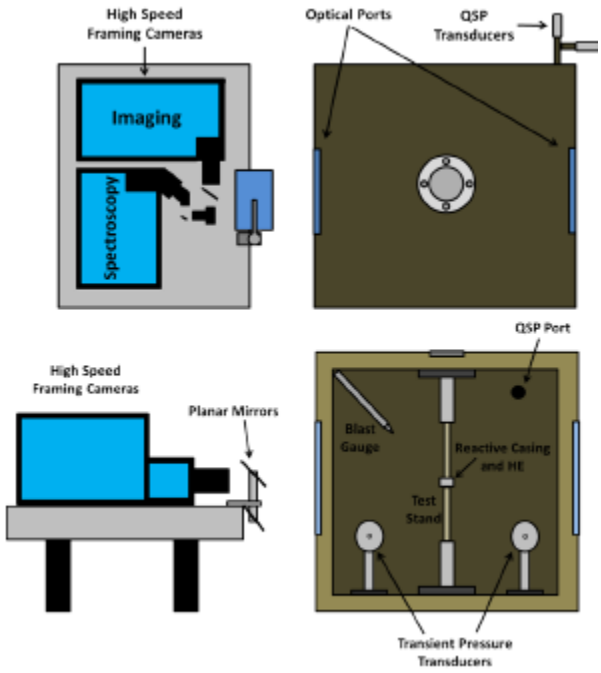

Figure 1.3: (Top) Top view of Clemenson setup, (Bottom) Front view of Clemenson setup

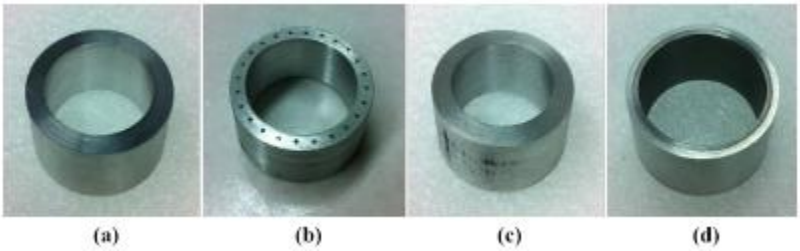

Figure 1.4: Cases tests by Clemenson: (a) Al 6061 baseline, (b) Axial holes filled with tungsten carbide rods, (c) Cast 5% lithium alloy, (d) Internal annulus steel confinement

1.4 Overview

This study parametrically investigates the top performing improvements from the study by M. Clemenson. From that research, the top performing alloy variation was the inclusion of magnesium and the top performing geometric variation was the inclusion of tungsten mesh in a cast aluminum case.

The objective is to find the maximum performance that can be achieved using these improvements. To accomplish this, a series of cases are made at the 40g scale and experimentally tested with 20g of HE representing a case mass to charge mass ratio of 2:1, similar to that of Clemenson. A series of baselines are tested in the form of bare charges, inert steel cases, and plain Al 6061 cases. The effect of magnesium alloying is investigated by testing cases with magnesium varying from 0 to 25% in 5% increments. Schematics of all variations are shown in Figure 1.5.

The effect of tungsten mesh is investigated by testing cases with 3 different mesh sizes as well as varying the number of wraps of tungsten mesh from 1 to 3.

Diagnostics consist of high speed imaging, piezoelectric pressure transducers, piezoresistive pressure transducers and will be discussed in detail in subsequent sections.

Casing mass, charge mass, end confinement, and ambient atmosphere are kept constant to isolate the effects of the chosen variations. Plywood veneers were added to the chamber walls on several tests to highlight the contribution of impact induced reaction (IIR) of fragments at the walls.

Manufacturing of reactive cases will be described in a later section and consists primarily of casting and machining. Scanning electron microscopy (SEM) was used to view defects from manufacturing. Tensile testing specimens of aluminum with tungsten mesh were fabricated to assess the effect of tungsten mesh in cast aluminum. Finally, conclusions are summarized and recommendations for future work are presented.

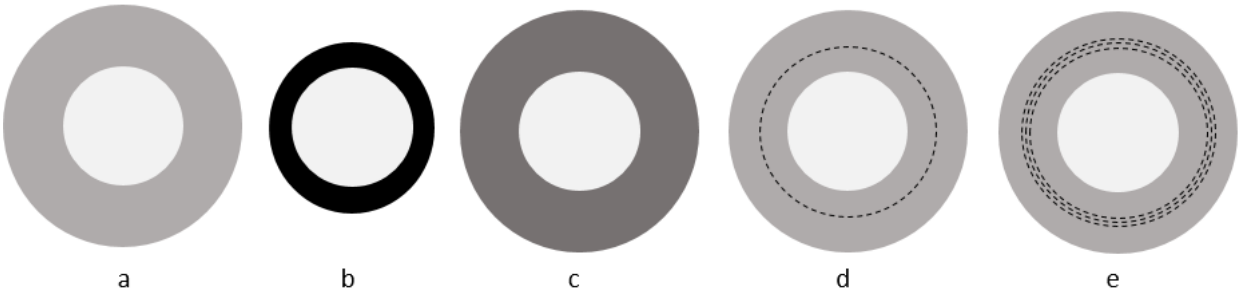

Figure 1.5: (a) Baseline Al 6061 configuration, (b) Baseline steel configuration, (c) Al/Mg alloy configuration, (d) Al with 1 wrap of tungsten mesh, (e) Al with 3 wraps of tungsten mesh

CHAPTER 2: EXPERIMENTAL METHODS

2.1 Reactive Casing Variation

A total of 29 tests were performed from March 2017 to November 2017. These include a bare explosive, an inert steel baseline, Al 6061 baselines, and the 3 parametric variations. All cases were machined to final dimensions with nominal height of 0.92 inches, inner diameter of 1.01 inches, and a mass of 40g. Because of the different case densities, the outer diameter slightly changed to maintain a constant mass of 40g. The constant mass constraint was implemented as opposed to something like constant dimensions in order to maintain a constant case mass to charge mass ratio (C/M) of 2 as the C/M parameter commonly appears as a non-dimensional parameter in fragmentation analysis. As previously discussed, the highest performing improvements to plain aluminum were alloying with magnesium and inclusion of tungsten. Naturally, these were selected for further analysis. The following subsections detail the parametric testing. A complete list of tests can be found in Appendix C. The HE used in all tests was 20g of PBXN-9.

2.1.1 Aluminum 6061 Baseline

Two baseline Al 6061 tests were performed. The case dimensions are shown in Table 2.1 and a photo is shown in Figure 2.1. Aluminum 6061 was chosen as the baseline because of its widespread use in engineering applications, good structural properties, and low cost. Cases were easily manufactured from commercially available tube stock with very little machining.

Table 2.1: Baseline Al 6061 cases

Height(in)	ID(in)	OD(in)	Weight(g)	Mg %	Mesh Size	# of Wraps
0.936	1.010	1.500	40.01	0%	None	None
0.925	1.012	1.500	39.90	0%	None	None

Figure 2.1: (L) Top view of baseline Al 6061 Case, (R) Side view of basline Al 6061 case

2.1.2 Magnesium Alloy Variation

Previous research has shown that when magnesium is alloyed with aluminum the ignition delay and ignition temperature of both are reduced [4]. It has been proposed that this is due to a two-stage combustion process in which magnesium burns first, then the aluminum, second. The magnesium combustion provides both additional heat and oxidizer at the liquid aluminum surface to improve aluminum combustion. However, magnesium has lower energy content per unit mass than aluminum which suggests the hypothesis for an optimum amount of magnesium that can be added to improve performance.

To find this optimum magnesium amount, cases were prepared using cast Al-Mg alloys ranging from 0% to 25% Mg. The 0% case representing Al 6061 baseline. Higher magnesium contents were not tested due to excessive oxidation in the casting process. The manufacturing process for all cases is described in more detail in a later section. Table 2.2 lists the cases that were tested.

Table 2.2. Cases varying magnesium

Height(in)	ID(in)	OD(in)	Weight(g)	Mg %	Mesh Size	# of Wraps
0.907	1.009	1.525	40.23	5%	None	None
.920	1.016	1.528	40.16	5%	None	None
0.951	1.007	1.502	39.98	10%	None	None
0.930	1.015	1.514	39.78	10%	None	None
0.891	1.006	1.540	39.91	15%	None	None
0.902	1.007	1.535	40.02	15%	None	None
0.922	1.011	1.554	40.26	20%	None	None
0.916	1.013	1.569	40.06	20%	None	None
0.912	1.010	1.555	40.00	25%	None	None
0.919	1.011	1.554	40.16	25%	None	None

2.1.3 Tungsten Mesh Variation

The goal for adding tungsten mesh to an aluminum case was to promote shock focusing in the mesh pattern as the detonation shock travels through the casing material. This is caused by the impedance mismatch of the aluminum matrix and tungsten wires [5]. The shock focusing generated points of higher temperatures and pressures than would otherwise be present as well as turbulent mixing during casing breakup. The effect of size and spacing of the wires was tested by embedding four different sizes of mesh. The meshes tested were size 18 x 18 wires per inch with 0.003” wire diameter, 30 x 30 wires per inch with 0.002” wire diameter, 50 x 50 wires per inch with 0.002” wire diameter, and 100 x 100 wire per inch with 0.001” wire diameter. All meshes use a plain weave pattern and were purchased from Unique Wire Weaving Co. Table 2.3 lists the cases that varied mesh size. The number of wraps of mesh were held constant at 2. In all cases the mesh was embedded at the midpoint of the case cross section.

The effect of the amount of tungsten mesh was also investigated by varying the number of wraps of tungsten mesh. Casings made with one, two, and three wraps of mesh were tested. These cases are listed in Table 2.4. Additionally a photo of the tungsten mesh and a fabricated case are shown in Figure 2.2.

Table 2.3. Cases varying tungsten mesh size

Height(in)	ID(in)	OD(in)	Weight(g)	Mg %	Mesh Size	# of Wraps
0.917	1.010	1.549	39.93	0%	18	2
0.926	1.013	1.521	40.11	0%	18	2
0.940	1.010	1.533	39.97	0%	30	2
0.931	1.012	1.530	40.28	0%	30	2
0.929	1.023	1.53	40.01	0%	50	2
0.925	1.021	1.54	40.06	0%	50	2
0.945	1.012	1.55	39.45	0%	100	2
0.916	1.01	1.55	40.16	0%	100	2

Table 2.4. Cases varying amount of tungsten mesh

Height(in)	ID(in)	OD(in)	Weight(g)	Mg %	Mesh Size	# of Wraps
0.939	1.016	1.520	40.00	0%	30	1
0.940	1.01	1.533	39.97	0%	30	2
0.931	1.012	1.530	40.28	0%	30	2
0.917	1.009	1.530	40.15	0%	30	3
0.915	1.008	1.543	40.20	0%	30	3

Figure 2.2: (L) Sample of tungsten mesh (R) Completed case with tungsten mesh

2.1.4 Effect of Impact Induced Reaction

It was shown by Clemenson that the addition of a layer of rubber mats to the walls of the blast chamber significantly reduces overall QSP. He concluded that a large fraction of the overall energy release was happening when high speed fragments broke apart and oxidized upon impacting the steel chamber walls. In this current study, three different wall materials are tested in addition to the baseline case of bare steel walls. The different wall materials were only tested with baseline

Al 6061 cases. The three wall setups chosen were 2 layers of 3/8” neoprene rubber mats, a single layer of 7/16” oriented strand board, and 2 layers of 7/16” oriented strand board. These materials were simply clamped on top of the normal steel fragmentation shields in the test chamber. Figure 2.3 shows the plywood setup on one of the chamber walls before and after a test.

Figure 2.3: (Top) Plywood layers before test, (Bottom) Plywood layers after test

2.2 Manufacturing of Reactive Cases

All cases were manufactured in house at the University of Illinois Urbana Champaign. Commercially available Al 6061 tube stock was purchased and turned on a lathe to create the 6061 baseline cases. Other cases were creating using one or more casting and machining steps. Figure 2.4 shows the casting lab setup. Commercially available tungsten meshes were purchased from Unique Wire Weaving Co.

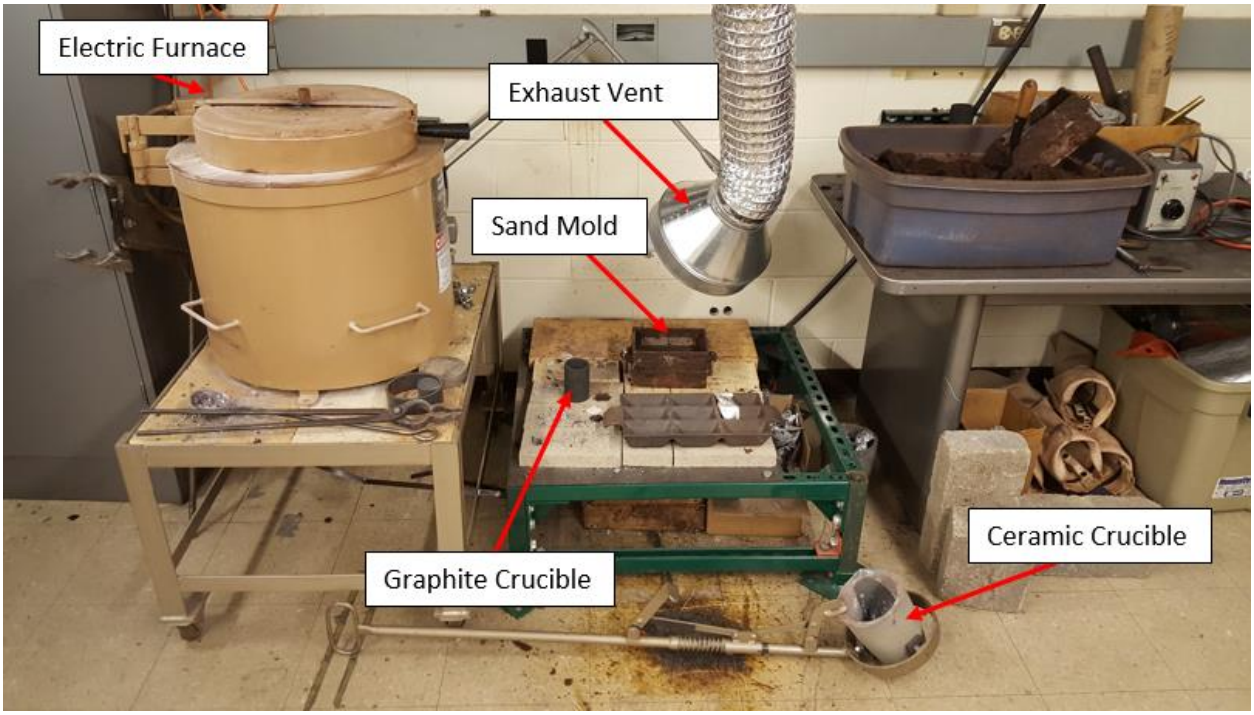

Figure 2.4: Casting lab setup

Cases with custom magnesium content were made by first weighing the appropriate amounts of Al 6061 and pure magnesium rods. The solid Al 6061 and magnesium pieces were then placed in a ceramic crucible with a small amount of casting flux added per the flux instructions of 1 tsp per pound of metal. The crucible was placed in the electric furnace and heated to 1400°F. Once melted, solid impurities and oxide were skimmed from the surface of the molten aluminum and the molten mixture was then poured into a sand mold to create a rough tube shape. An example of a cast tube is shown in Figure 2.5. The rough casting was then turned on a lathe to final dimensions or machined into an inner or outer annulus for manufacturing of a meshed case.

Figure 2.5: (L) As cast Al/Mg tube, (R) Machined inner and outer annuli

Cases with tungsten mesh inclusions were created using a multistep process. First, two tubes were cast in the manner previously described. The two annuli were made such that they could fit concentrically with tungsten mesh wrapped in between. A graphite rod was inserted in the middle and placed in a graphite crucible. The assembly, shown in Figure 2.6, was then placed in the furnace at 1400°F to melt and infiltrate the tungsten mesh. Once removed from the furnace and cooled, the graphite rod was pressed out with a hydraulic press, and the case machined to final dimensions.

Figure 2.6: (L) Graphite crucible and annuli with tungsten mesh wraps inserted, (R) Assembly ready to be placed in furnace for infiltration

2.3 Experimental Setup

The experimental setup consists of a 4 foot cube chamber with 6 pressure transducers as well as a high speed framing camera. A schematic of the setup is shown in Figure 2.7. Two of the pressure transducers are PCB piezoelectric pressure transducers (Part no. 137B23B) shown in Figure 2.8. A piece of electrical tape is placed over the sensing element to provide thermal insulation from flash heating per the user manual [6]. Because of the fast response time, the PCB piezoelectric pressure transducers are used for characterizing the peak blast pressure and impulse. Piezoelectric sensors cannot be used for QSP measurement, since those only measure dynamic pressures. Calibrations for these transducers came from the manufacturer. In this study the probes were mounted in the diagonal plane of the cube pointed at the charge in the center such that the sensing elements were located 24", approximately 16 charge diameters, from the charge center for all tests.

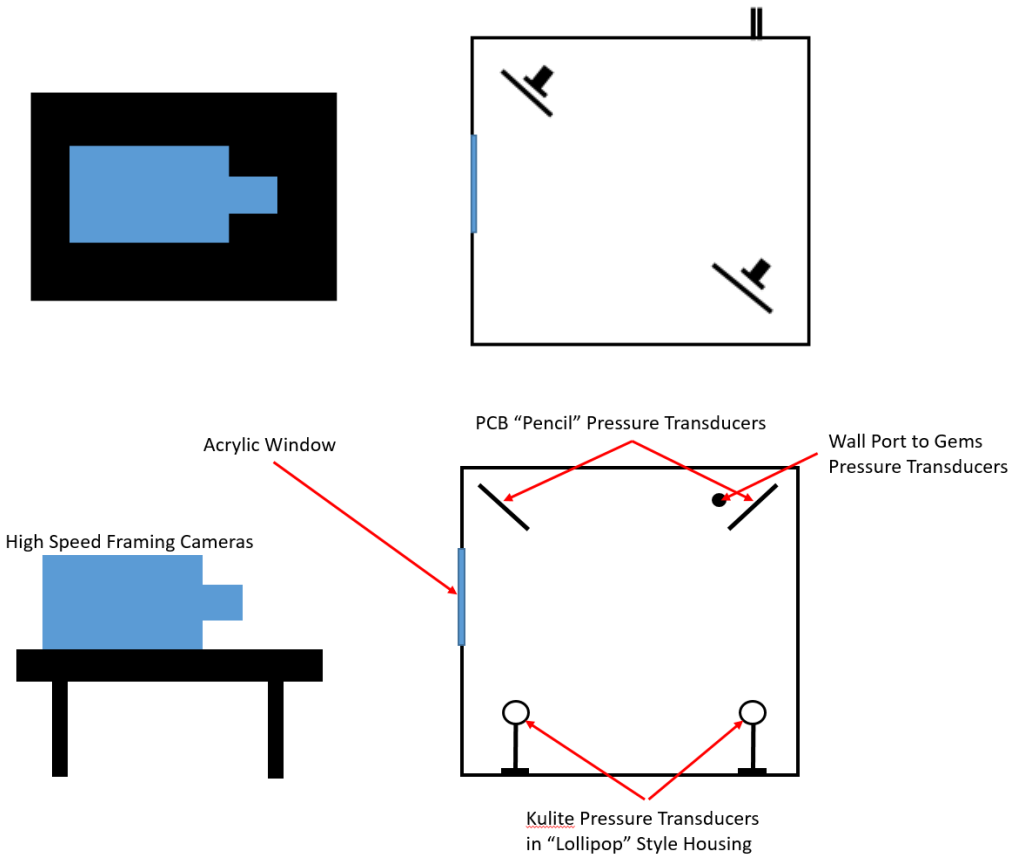

Figure 2.7: (Top) Chamber schematic top view. (Bottom) Chamber schematic side view

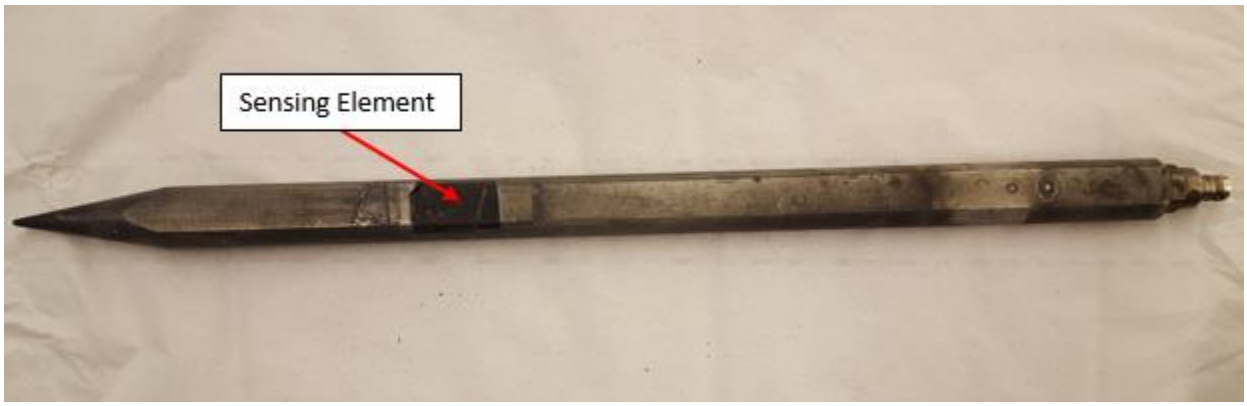

Figure 2.8: PCB Piezotronics 137B23B piezoelectric pressure transducer

Two Kulite piezoresistive pressure transducers (XTEL-190A) are also installed in the test chamber. A transducer in its lollipop style housing is shown in Figure 2.9. The lollipop style housings are affixed to posts on magnetic mounts located on the floor of the chamber in the same diagonal plane as the pencil probes. The lollipop housings are oriented edge-on in order to "cut" the blast wave and obtain a clear measurement. Again, the transducers are arranged such that the sensing elements are located 24" from the charge center. The Kulite pressure transducers are used for blast as well as QSP measurements.

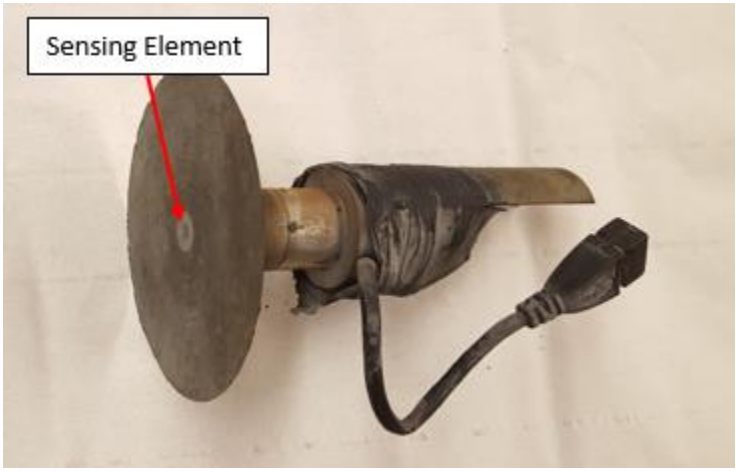

Figure 2.9: Kulite XTEL-190A pressure transducer in lollipop style housing

Two Gems #2200 series pressure transducers are mounted outside the chamber and connected via stainless steel tubing. An image of one of a Gems #2200 series pressure transducer is shown in Figure 2.10. Because of the slow response time and the indirect line of sight to the charge, these sensors are used only for the QSP measurement. Due to their ability to be statically calibrated, the

Kulite and Gems transducers in this study were recalibrated regularly by sealing the chamber and pressuring to known values, while recording the voltage output to create a linear regression. Example calibration data is provided in Appendix Table A.1. Data from all pressure transducers was recorded using digital oscilloscopes from Pico Technologies (Model 3424) with an example shown in Figure 2.10.

Figure 2.10: (L) Gems #2200 series pressure transducer (R) Pico Technologies Oscilloscope Model 3424

The PCO Technologies high speed framing cameras (HSFC) provide 4 images of each detonation event. Timing and exposures can be accurately controlled. For this study a variety of timings were used and exposures were set to 60 nanoseconds. The images provide a qualitative look at early time breakup, confinement, and asymmetries. An example series of images is shown in Figure 2.11.

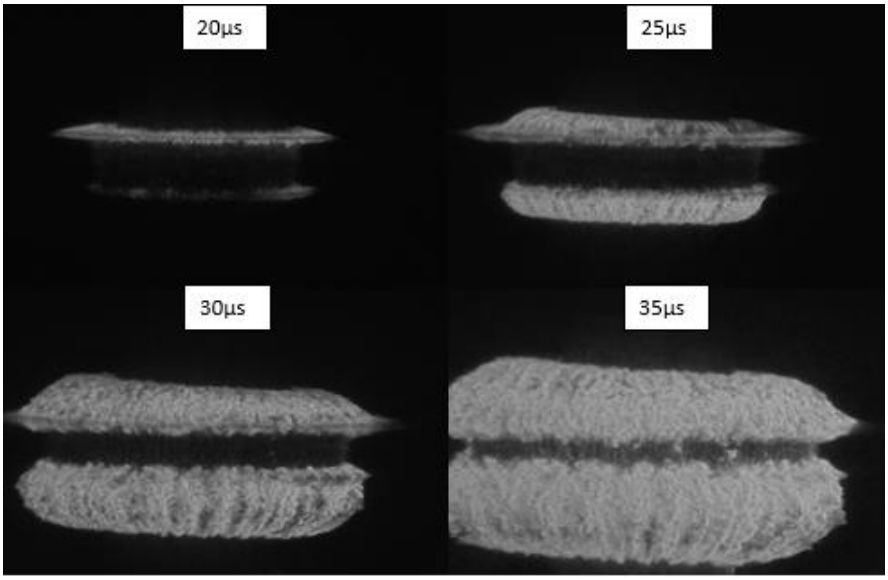

Figure 2.11: Typical HSFC image series

M. Clemenson found that end confinement of the annular test articles was found to have a significant effect on the performance of reactive cases. Therefore a mostly reusable heavy-duty confinement setup was designed and built to consistently provide a clamping force on the ends of the test article. Additionally it was desired that the confinement setup be independent of the chamber floor and ceiling. A schematic of the heavy confinement setup is shown in Figure 2.12. The structure consists of a base plate, two vertical side posts, and a beam across the top. When a charge is placed, the clamping bolt at the top of the setup can be turned to compress the spring and apply pressure on the test article held between two steel anvils. The anvils and low density polyethylene (LDPE) spacers are replaced for every test. The rest of the structure is reused. Engineering drawings of the parts are provided in Appendix B.

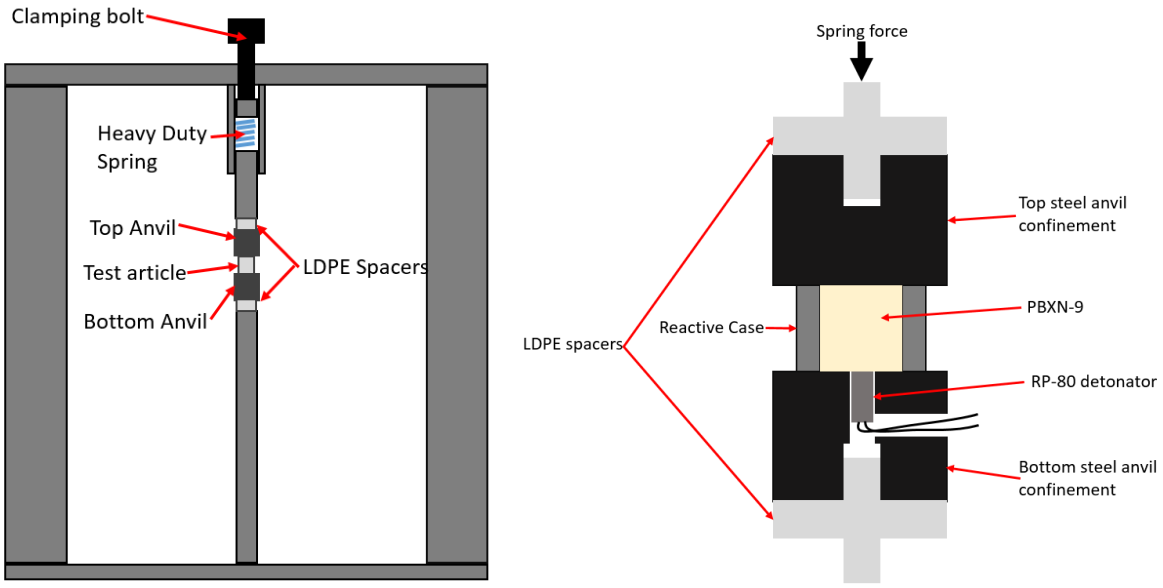

Figure 2.12 (L) Side view of heavy confinement setup. (R) Detailed view around charge

CHAPTER 3: RESULTS AND DISCUSSION

3.1 Pressure Data Reduction

Pressure data was analyzed using MATLAB. Typical pressure time traces for each type of transducer are shown in Figures 3.1, 3.2, and 3.3. The processing code used can be found in [7]. Reported QSP values were averaged across the 4 relevant transducers (2 Gems and 2 Kulite). Reported impulse values are averaged from the 2 Kulite transducers. Reported blast pressures are averaged from the 2 pencil probes. Additionally, 2 tests of each casing configuration were tested.

As previously mentioned, QSP (ΔP) can be used to calculate total energy release. Using the ideal gas law, the temperature increase (ΔT) associated with the chamber overpressure can be calculated. It is assumed that the gas in the chamber is ideal and of known composition. It is also assumed that the volume of the detonation products of 20g of PBXN-9, which is 92% HMX, are insignificant compared to the chamber volume of V = 1.775m^3.

$$\Delta PV = nR\Delta T \tag{3.1}$$

The temperature change can be used to calculate the energy output of the reaction using Equation 3.2. The value of the constant volume specific heat, c_v, is assumed to be constant and the value chosen is that of air at STP. The assumption that c_v is constant is relatively good, since it changes by only a few percent over the ΔT ranges involved in this study. An integral analysis could be performed if further accuracy is desired. Another assumption made in this analysis is that heat loss to the chamber walls and solid products is negligible over the timescale of interest (~100ms). The total energy released can then be divided by the case mass or combined case plus charge mass in order to calculate the specific energy output of the test, a common metric for energetic materials.

$$E = mc_v\Delta T \tag{3.2}$$

For relative comparison between tests, QSP will be used as it is directly proportional to energy release as well as specific energy given that the charge and case mass were nominally the same for all tests.

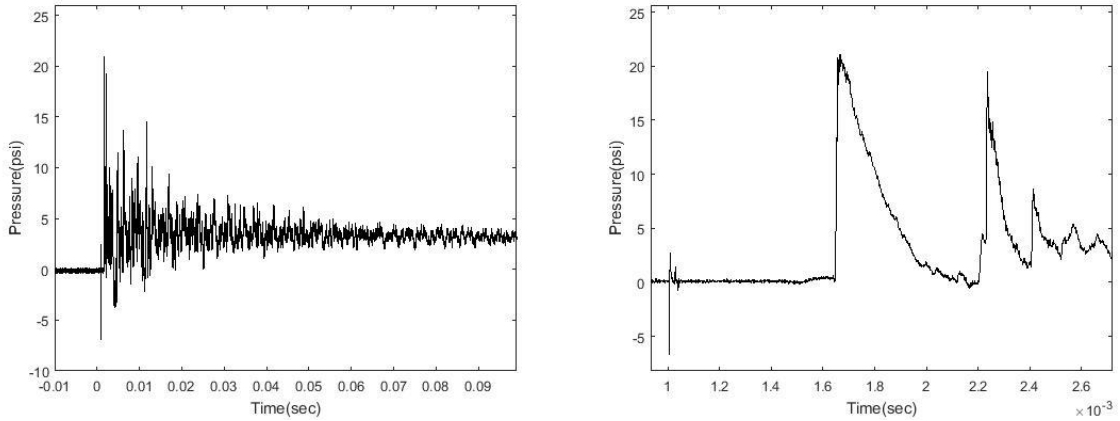

Figure 3.1: (L) Complete pressure vs time trace for a PCB pencil probe, (R) Zoomed in on first positive phase

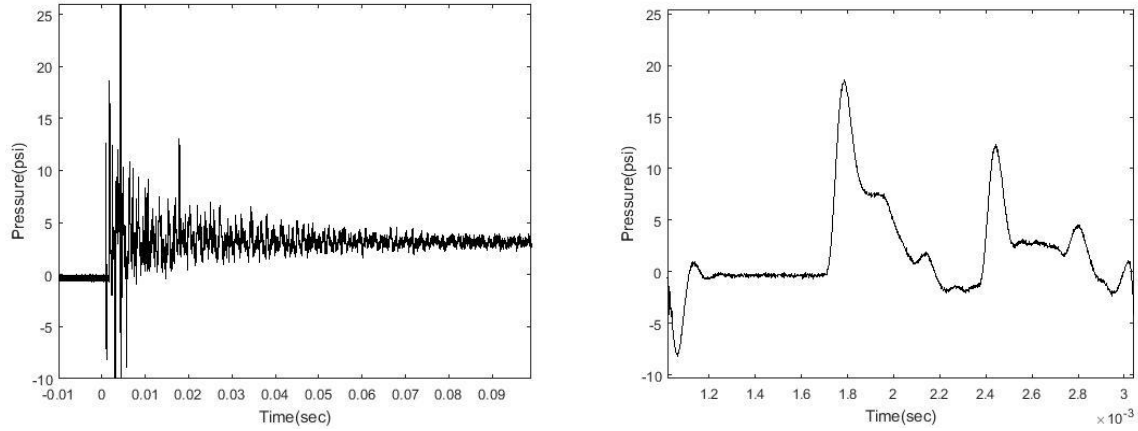

Figure 3.2: (L) Complete pressure vs time trace for a Kulite pressure transducer, (R) Zoomed in on first positive phase

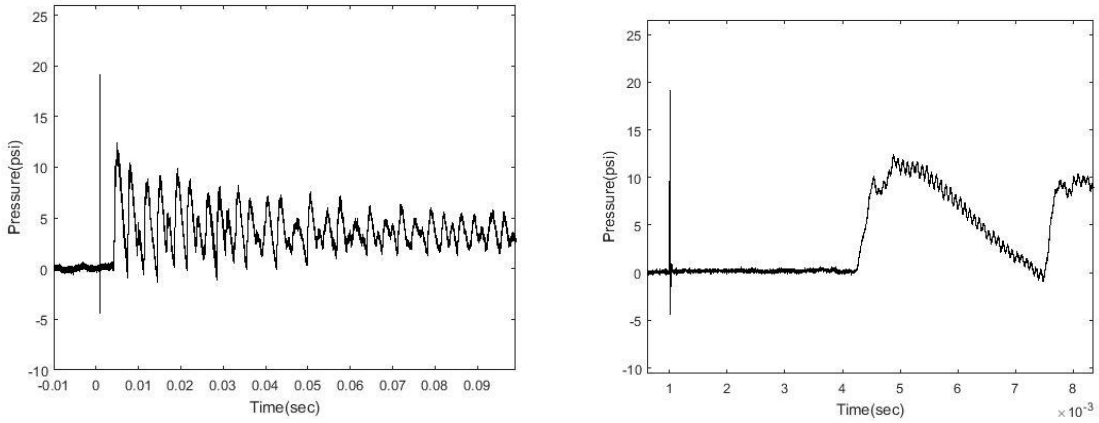

Figure 3.3: (L) Complete pressure vs time trace for a Gems pressure transducer, (R) Zoomed in on first positive phase

3.2 Varying Magnesium Content

The results of varying magnesium content are shown in Figures 3.4, 3.5, and 3.6 alongside baseline data from bare HE, an inert steel case, and plain Al 6061 baselines.

Consider first the baseline results. It can be seen that bare HE has very high blast and impulse characteristics, but relatively low QSP. This is because bare HE releases its energy very quickly (microseconds) with all the energy contributing to the shockwave. Additionally, the shockwave is not impeded by any case mass. Using the energy analysis previously described, a total energy release of 108 kJ and a specific energy release of 5.40 kJ/g are calculated. This is ~3% above the theoretical value of detonation enthalpy for PBXN-9, based on its 92% HMX content. The plastic binder is known to burn and is unaccounted for in this simple analysis. This is likely what contributes to the slightly higher than expected energy release.

Low carbon steel represents a typical inert steel casing. For the low carbon steel case it is expected that all characteristics are lower due to energy being expended in fracturing the steel and accelerating the fragments. Indeed it is observed that QSP is reduced 43%, peak blast pressure is reduced 42%, and impulse is reduced by 36%.

The baseline Al 6061 cases show slight improvements in peak blast pressure and impulse compared to steel. This is likely due to a combination of less energy expended in fragmenting the case as well as some energy release from early reactivity of the fragments. Still, peak blast pressure and impulse are much lower than that of bare HE. QSP shows an improvement of 177% compared to bare HE. Following below, we see that most of this energy is released when high speed fragments impact the chamber walls. This is known as impact induced reaction (IIR). Based on the QSP, the energy release is calculated to be 276 kJ. Subtracting the energy release previously measured for a bare charge leaves 168 kJ contributed by aluminum combustion giving a specific case energy release 4.2 kJ/g of case material. This represents 13.5% combustion of the 31 kJ/g potential present in aluminum.

The addition of any amount of magnesium shows improvements in all metrics over the baseline aluminum case. It appears that peak performance for all metrics occurred for the 20%/80% Mg/Al alloy indicating that this is the optimal ratio. For the 20% case, QSP is increased over the baseline by ~99%, peak blast pressure is increased by 53%, and peak impulse is increased 48%. The greater

QSP is mostly attributed to reaction at the walls, but at least some prompt reactivity must be occurring in order to improve the blast and impulse metrics. The enhanced blast and impulse are recovered to approximately the same level as the bare charge for the best performing alloys. Agreement between duplicate tests is relatively good for QSP, but suffers slightly for blast and impulse measurements due to higher signal noise during the initial blast wave as well as local transient effects. Still, a trend is clear. An example of asymmetry that could lead to inconsistent blast measurements is shown in Figure 3.7. The circled feature could have been caused by a defect in the casting process.

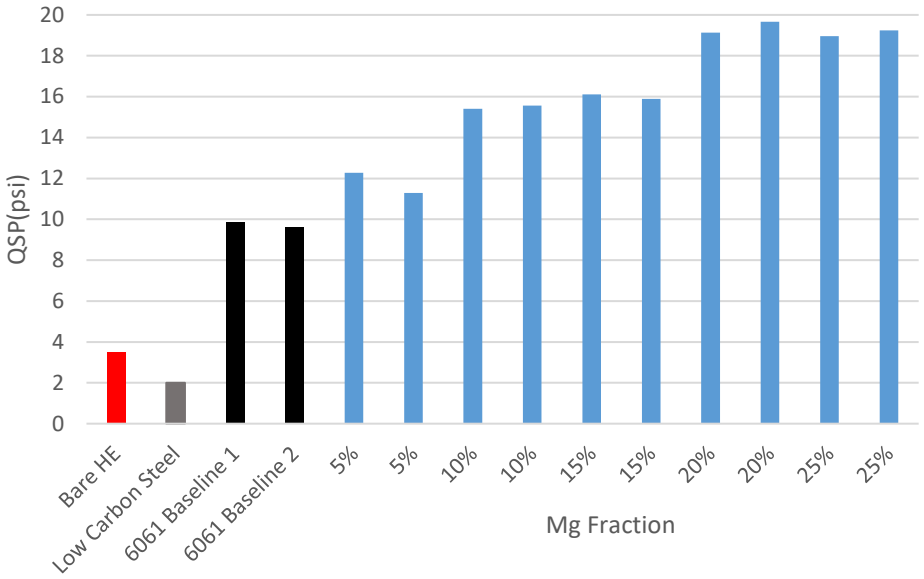

Figure 3.4: QSP vs. Mg Fraction

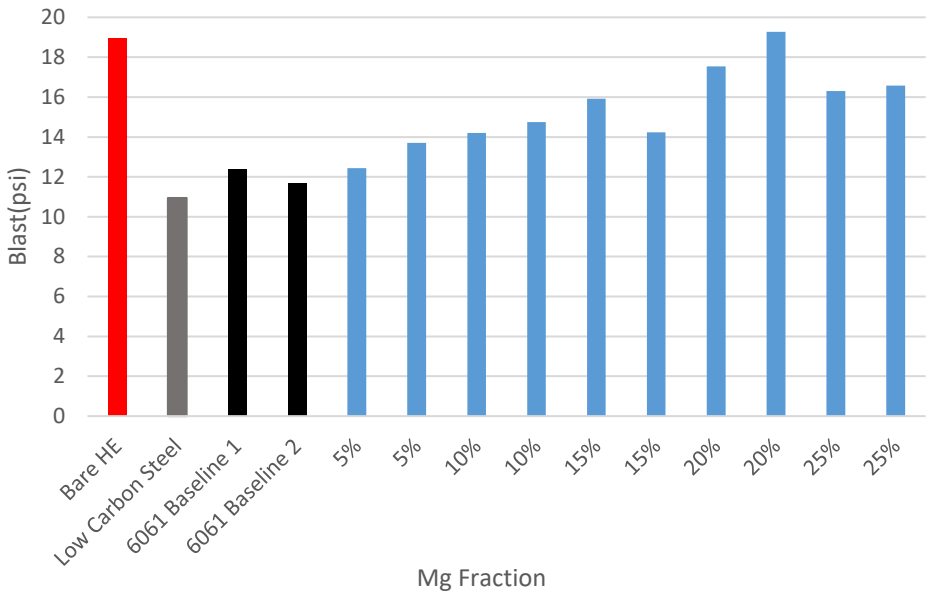

Figure 3.5: Peak blast pressure vs. Mg Fraction

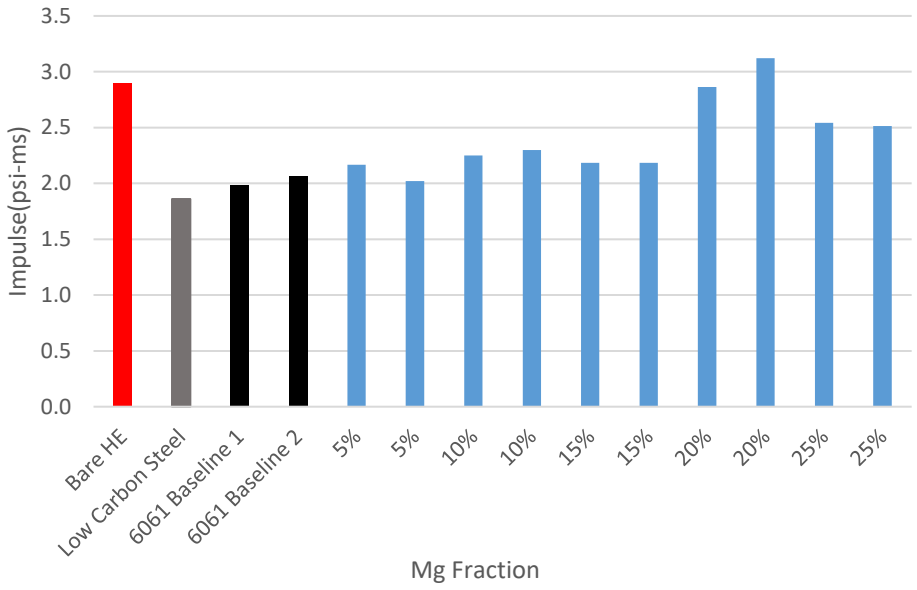

Figure 3.6: Impulse vs. Mg Fraction

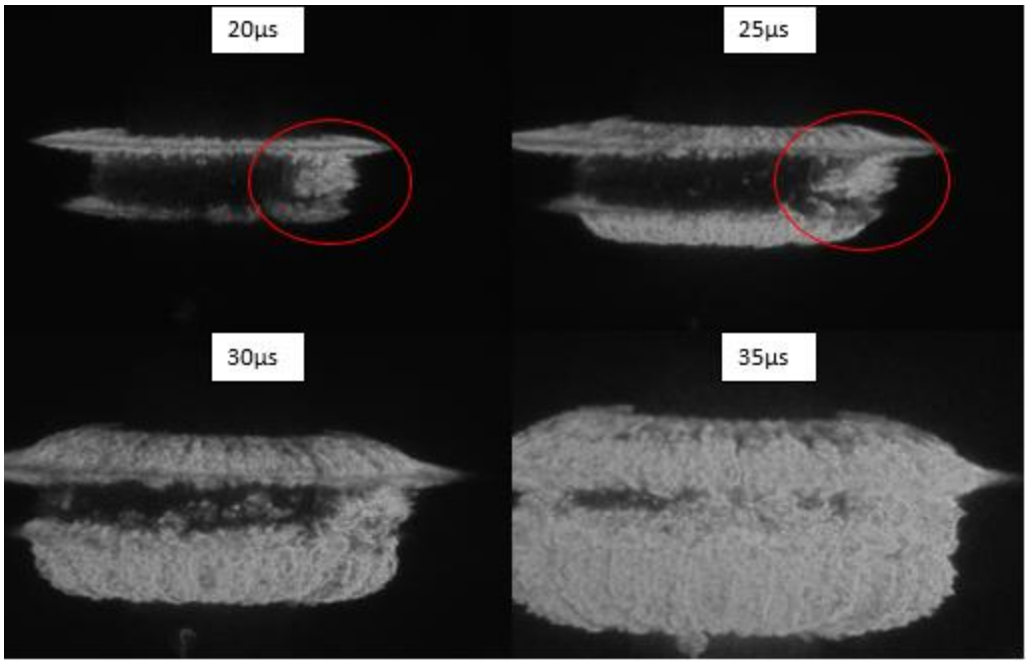

Figure 3.7: Asymmetry in breakout caused by manufacturing defect

3.3 Varying Tungsten Mesh Size

Figures 3.8, 3.9, and 3.10 show the results when adding 2 wraps of tungsten mesh of varying sizes to cast aluminum cases. The data for duplicate test cases are noticeably less consistent than for the Mg test variations. This is attributed to the likelihood of manufacturing defects when casting around tungsten mesh. The high surface tension of liquid aluminum can lead to lack of infiltration of the mesh structure. The lack of infiltration can also leave air gaps within the case material, which can asymmetrically affect shockwave impedance, case combustion, and subsequent pressure measurement consistency.

It's difficult to identify an optimal mesh given the inconsistency, but an important trend can still be made: any included mesh improves all the measured blast characteristics. QSP is increased by at least 50% for all mesh sizes. Peak blast pressure is increased by at least 17% for all mesh sizes. Impulse is increased by at least 6% for all mesh sizes. Individual tests show improvements as high as 80% for QSP, 42% for peak blast pressure, and 50% for impulse. More tests and a more consistent manufacturing process are recommended for a more conclusive discussion.

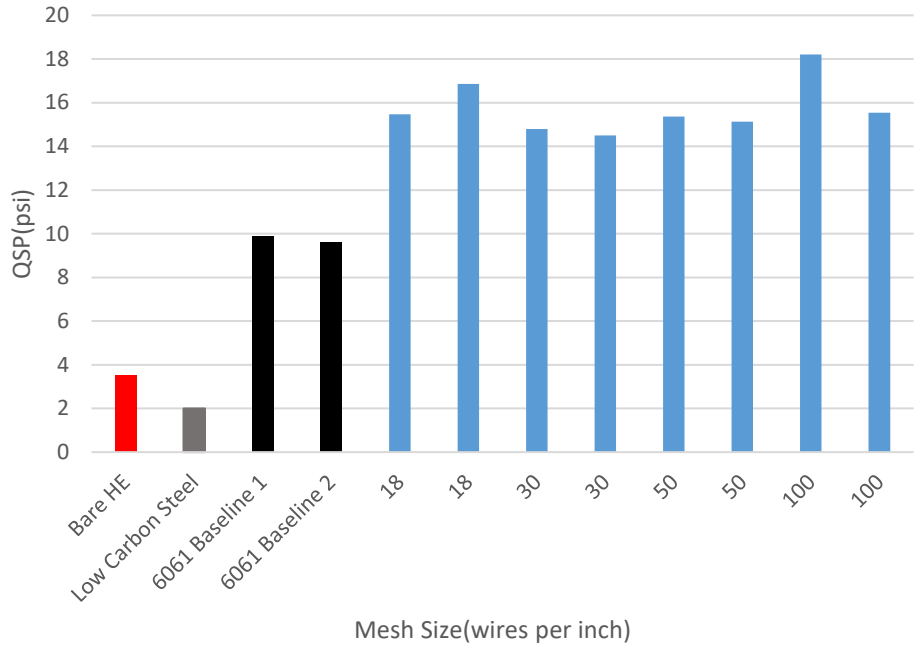

Figure 3.8: QSP vs. Mesh size

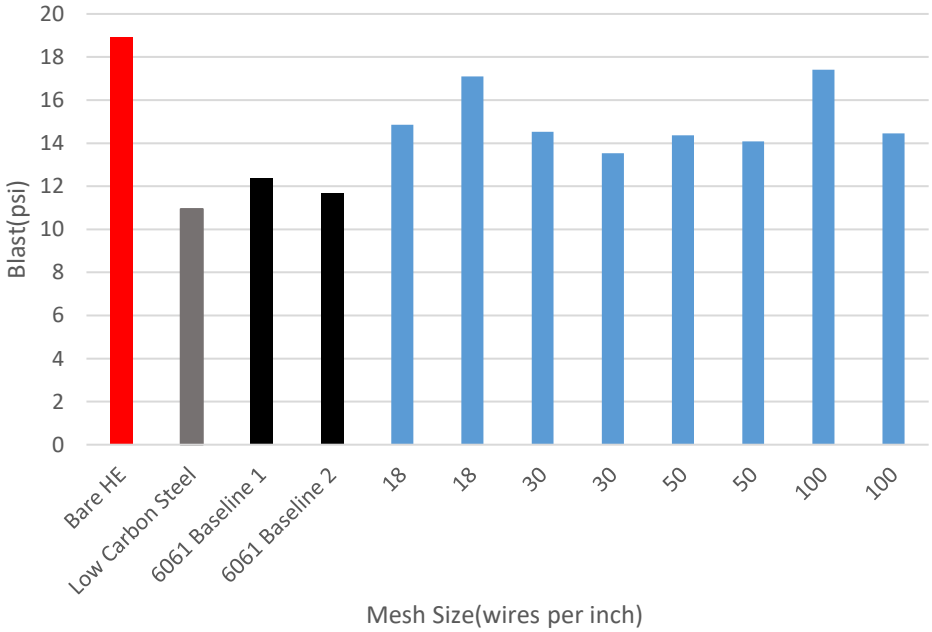

Figure 3.9: Peak blast pressure vs. Mesh size

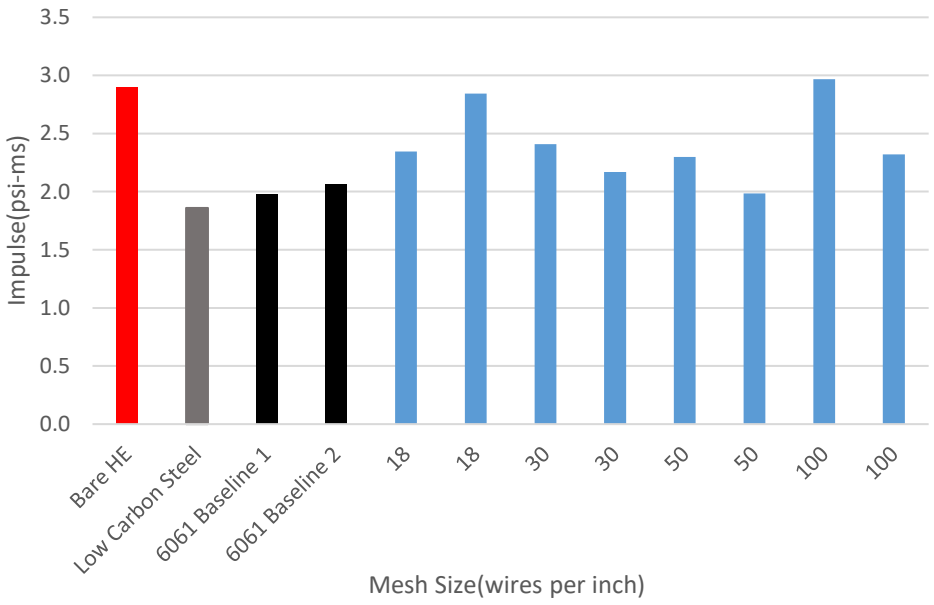

Figure 3.10: Impulse vs. Mesh size

3.4 Varying Number of Wraps of Tungsten Mesh

Figures 3.11, 3.12, and 3.13 show the results of adding 1, 2, or 3 wraps of size 30 mesh to the cast aluminum cases. Similar to the previous section, the data are less consistent due to inconsistencies in the casting and infiltration steps of casing fabrication. Even so, the same observation holds true: any amount of added mesh shows improvements in all blast characteristics over the Al 6061 baselines. QSP improvements range from 50% to 60%. Peak pressure improvements range from 10% to 35%. Impulse improvements range from 10% to 28%.

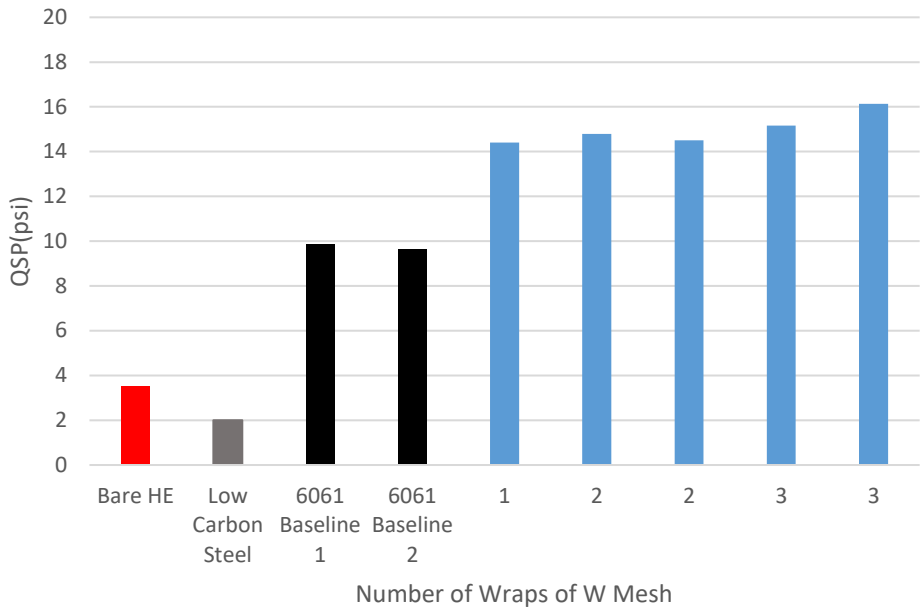

Figure 3.11: QSP vs. Number of wraps of mesh

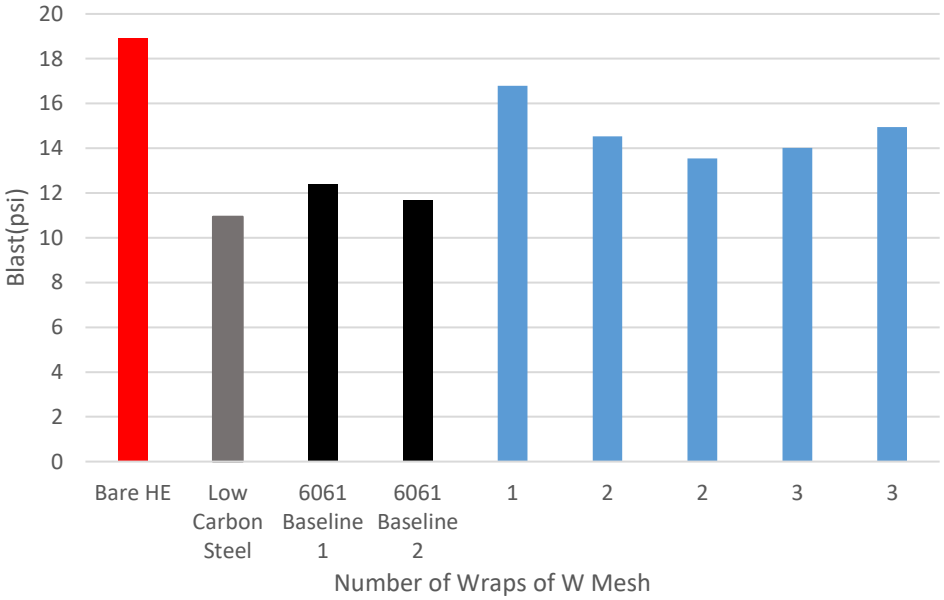

Figure 3.12: Peak blast pressure vs. Number of wraps of mesh

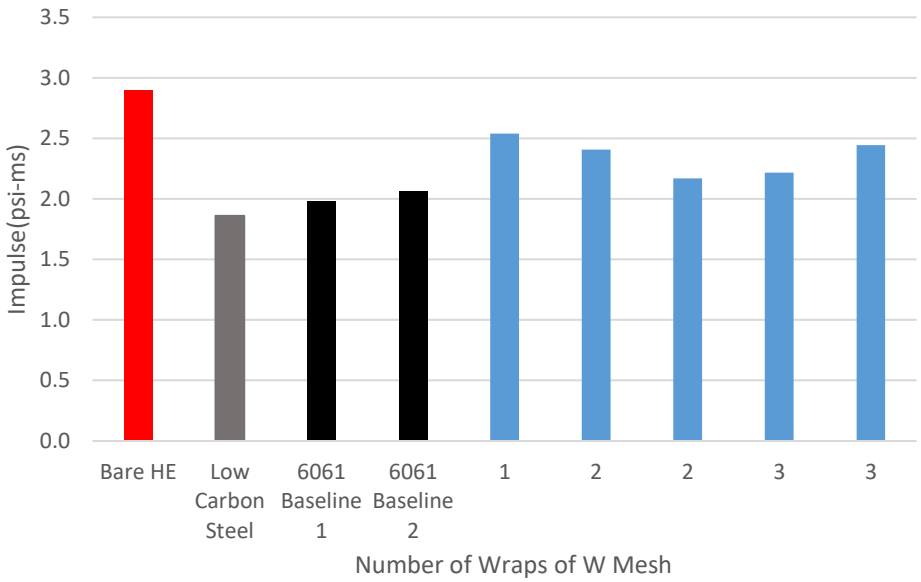

Figure 3.13: Impulse vs. Number of wraps of mesh

3.5 Contribution of Impact Induced Reaction

Figure 3.14 shows the results of varying chamber wall material. In theory, adding a more shock absorbing material to the chamber walls should only affect the QSP, due to changing late time fragment reactivity at the walls. The early time blast characteristics of peak blast pressure and impulse should be unaffected. This is exactly what was experimentally observed. Blast and impulse measurements for various wall materials are within the shot to shot variation of the baseline tests, while the QSP is reduced by as much as 80% in the case of 2 plywood layers to the same level as that measured for an inert steel case.

This indicates that almost all extra energy contributed by an aluminum case in a sealed test chamber is due to fragments reacting at the walls. The fact that blast and impulse measurements are still slightly above the steel baseline indicates there may be some early time reactivity or simply less impedance to the shock wave due to the lower density of aluminum compared to that of steel.

For the tests with rubber mats and one layer of wood, QSP values are still above the inert baseline. This indicates that there is partially suppressed but not fully inhibited reaction at the chamber walls. For any future testing of IIR at least two 7/16” wood panels are recommended. The effect of IIR were not quantified for the alloy or mesh cases and could be investigated in the future. It is

likely that a large portion of the QSP enhancements seen in the previous data would be suppressed with the use of wood panels, while the more modest blast enhancements would remain.

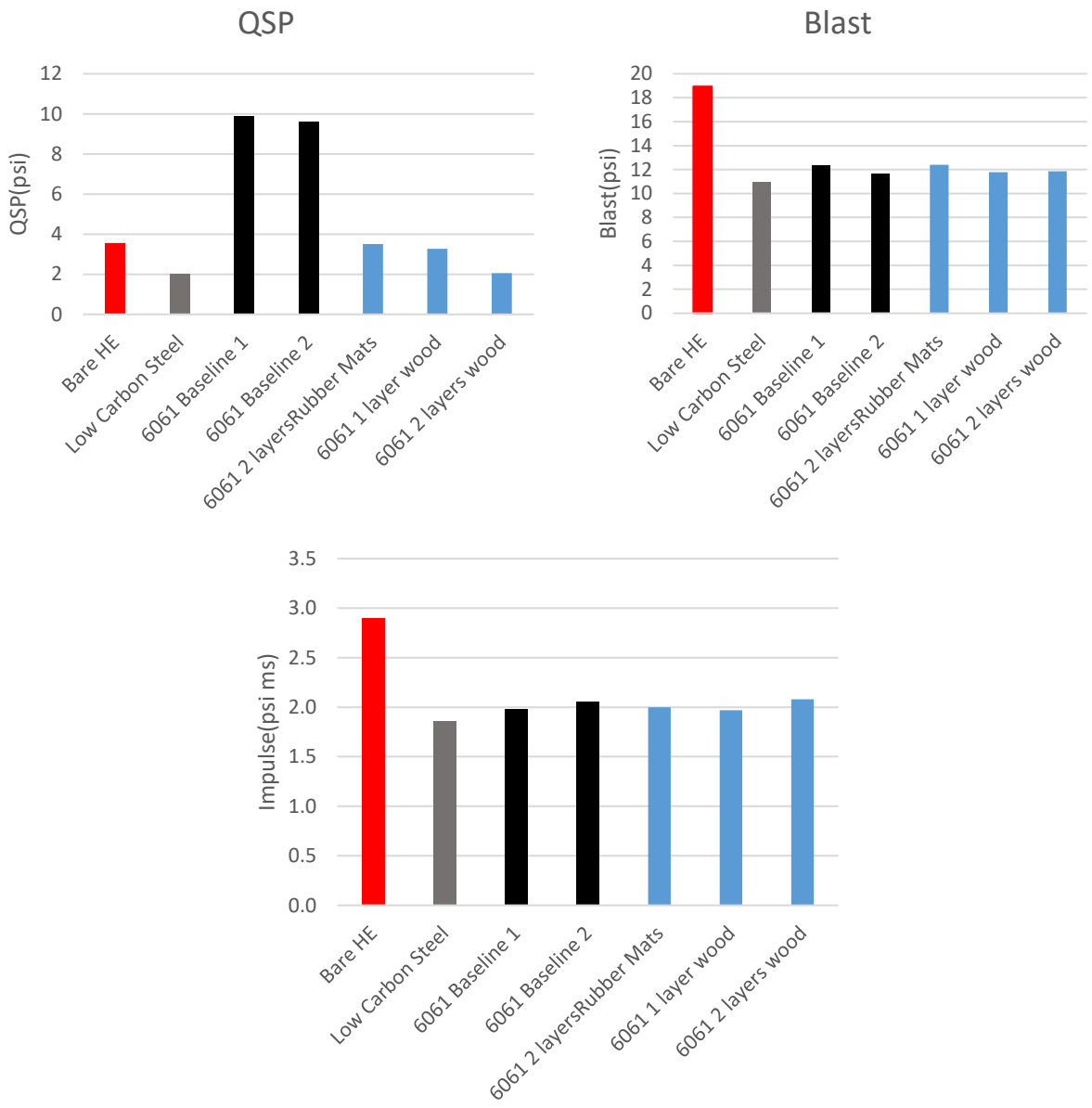

Figure 3.14: (Top Left) QSP, (Top Right) Blast pressure, (Bottom) Impulse for varying wall material

3.6 Top Performing Casing Variations

Two casings outside of the previous parametric test series were tested. The first was a 20% Mg alloy, similar to what was previously tested, but with a slight difference in manufacturing. Instead

of melting the magnesium bars together with the aluminum, the magnesium bars were added to the molten aluminum at the end of the melting process and just prior to pouring in the mold. This was done to reduce the amount of magnesium lost to oxidation in the furnace environment.

The results of this alteration are shown in Figure 3.17. This simple change led to a an increase in QSP of 11%, and increase in peak blast pressure of 28% and an increase in impulse of 11% compared the same alloy composition with magnesium added earlier in the melting process. This indicates that the previous alloy variations may all have suffered from loss of magnesium. The absolute accuracy of the optimum alloy composition in the previous data likely contains some error, but the data would not have changed, as they were all manufactured with the same procedure. In the future, casting could be done under an inert atmosphere to avoid the issue of premature magnesium oxidation.

The second case tested outside the previously mentioned parametric variations was designed to combine the previously tested geometric and alloy effects to create a top performing case. Trends in the previous data indicated that 20% Mg was the optimum alloy composition. The magnesium was added at the end of the melting process as that had just been shown to affect performance. Additionally, 3 wraps of size 18 mesh were embedded. The choice of mesh size and number of wraps likely were not critical as any mesh has been shown to improve combustion performance. Finally, a case was manufactured with the three wraps of mesh at three separate radial locations as opposed to all stacked at the same location. This required multiple steps of casting and machining to add layers to the case. The finished product is shown in Figure 3.15. The three distinct layers of mesh are visible, as well as some spots where infiltration did not occur well. This case ended up being the top performing case in the study owing to the combination of alloy and geometrical enhancements.

The results shown in Figure 3.17 show a 123% improvement in QSP, a 105% improvement in peak blast pressure, and a 102% improvement in impulse compared to the baseline Al 6061 case. Using the energy analysis discussed previously, the total energy release of the system was 675kJ while the bare charge released only 108kJ. *The difference in energy release of 567kJ is attributed to the casing combustion, more than 5x the energy release of the HE itself*. Furthermore, the peak blast pressure and impulse recovered are significantly greater than that of a bare charge, negating

the performance decrease associated with the presence of case material. Figure 3.16 shows the first positive phase of the blast wave overlaid for several selected tests. This figure clearly illustrates the higher performance (higher peak pressure as well higher overpressure throughout the positive phase) of modified reactive aluminum/magnesium cases compared to a baseline aluminum case as well as bare HE.

Figure 3.15: Cast case with 3 separate layers and Mg alloy

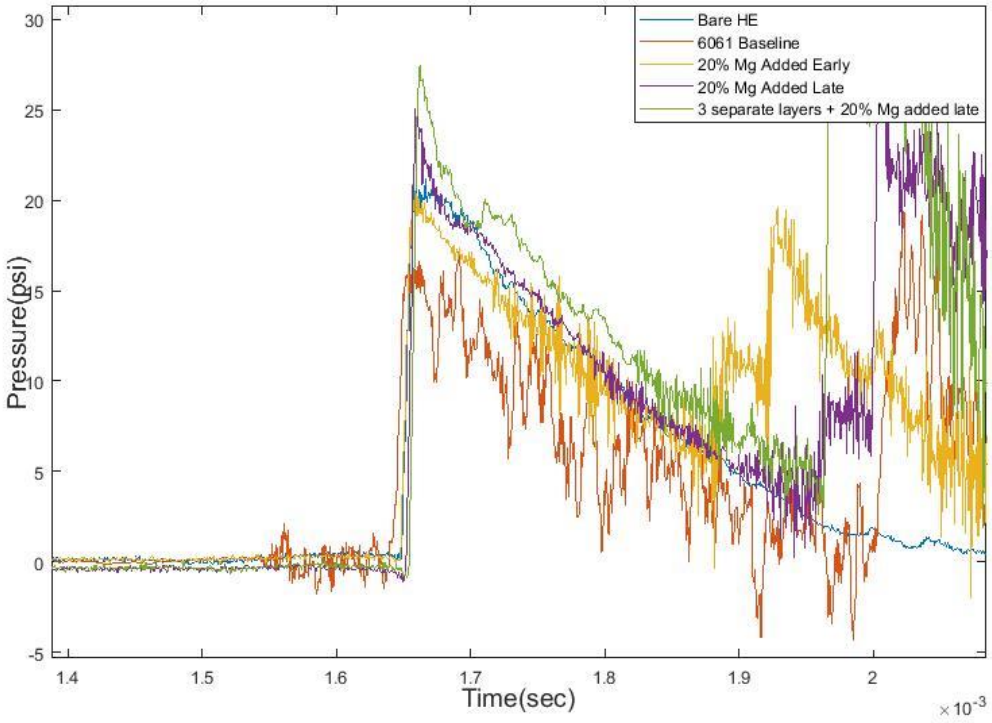

Figure 3.16: Initial blast wave pressure traces of select cases

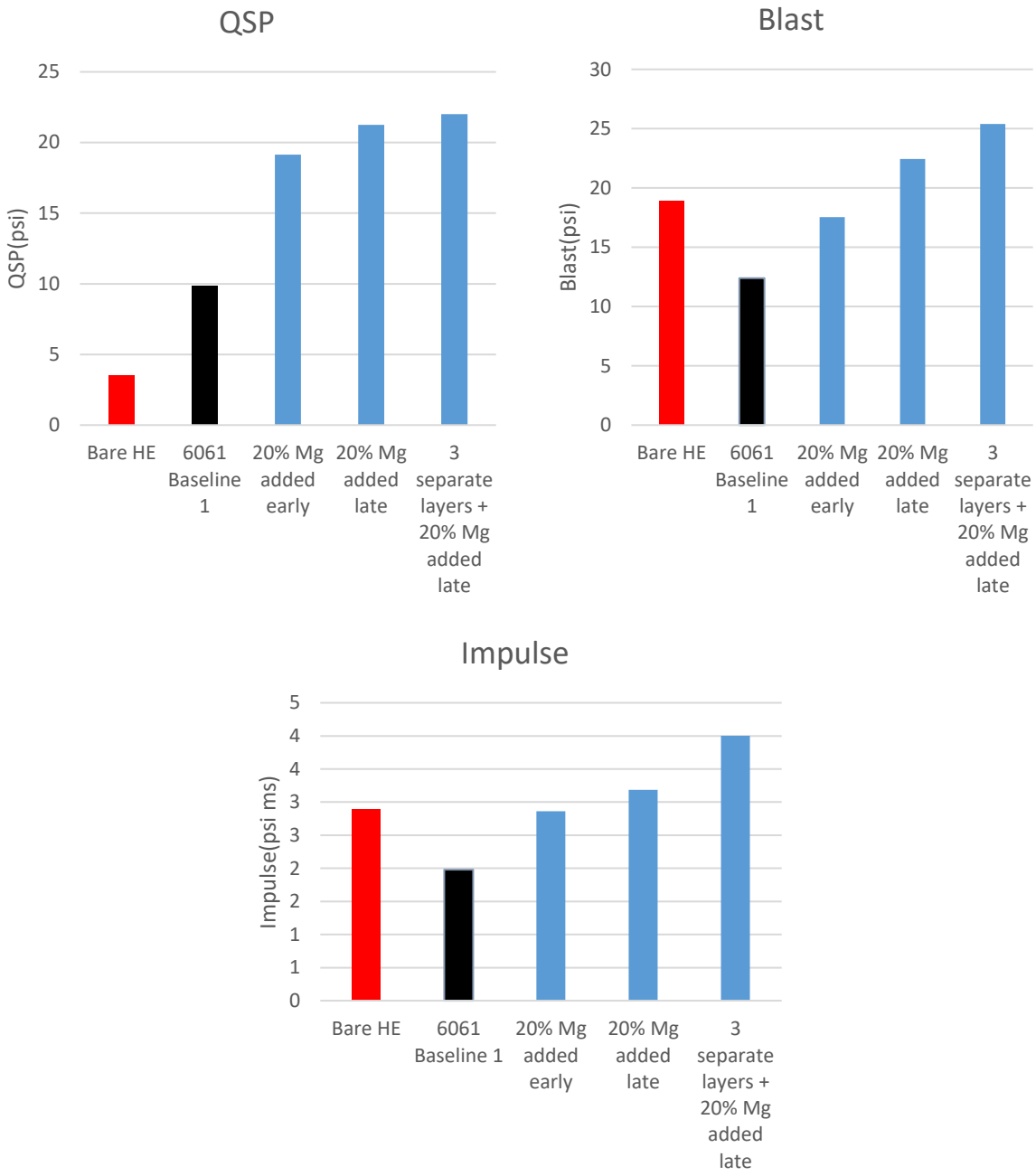

Figure 3.17: (Top Left) QSP, (Top Right) Blast pressure, (Bottom) Impulse for cases outside the parametric test series

3.7 Material Testing

Tensile tests were performed on samples of Aluminum alloy 356 with and without embedded tungsten mesh to see if the energetic enhancement of tungsten mesh compromises the structural

properties. “Dog bone” tensile specimens were cast with a single layer of size 18 mesh embedded at the midpoint. The rough castings were ground flat and then wire EDM cut to final dimensions. The dimensions of the test specimen can be found in Appendix Figure B.11 and follow the ASTM E8 standard for a flat tensile specimen. All specimens were tested in the as-cast state. That is to say they were not heat treated, aged, or precipitation hardened in any way. This is not typical for an engineering application of aluminum, but it provides a convenient and consistent baseline to compare different specimens. A tested specimen is shown in Figure 3.18. The single layer of mesh is visible throughout the specimen.

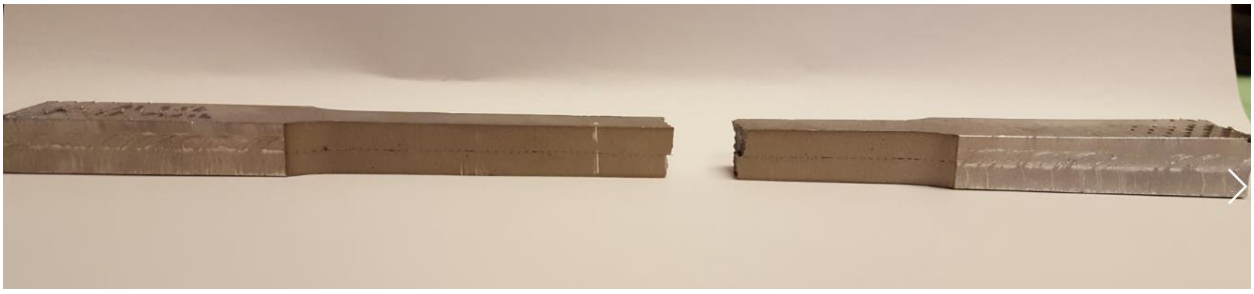

Figure 3.18: Tensile test specimen after testing

Tensile tests were performed on the 120,000-lb Riehle tension/compression machine located in Talbot Laboratory here at the UIUC. The machine is annually calibrated by Professor Emeritus James Phillips to within 1% accuracy overall all load ranges. The stress-strain curves from 4 specimens are shown in Figure 3.19 with material properties summarized in Table 3.1. Properties are averaged from the two tests of each type.

It can be seen that cast specimens perform worse than published values for Al 356 alloy. It’s possible there are systematic quality issues in the lab casting process such as gas absorption or oxide formation, resulting in the low values compared to commercial processes. Even so, the cast specimens without mesh can be used as a baseline for comparing specimens with embedded tungsten mesh. Doing this, it can be seen that embedded mesh slightly decreases elastic modulus, increases elongation at break, and increases ultimate strength. The strength of tungsten itself does not account for this increase in strength and ductility (the cross sectional area of the mesh is on the order of 1% of the test specimen). It is possible that the presence of the mesh during casting provides grain nucleation sites for solidifying aluminum. This could lead to a finer grain structure and therefore improved properties. It is also possible that incomplete infiltration of the mesh could

lead to air bubbles in the specimens, leading to a smaller effective cross sectional area which would contribute to the lowered elastic modulus. A larger sample size as well as microstructure analysis would yield more insight in future studies. Overall, the materials properties of A356 aluminum with embedded tungsten mesh are not worse than A356 aluminum without mesh. In fact, based on initial testing, tungsten inclusions could strengthen the material.

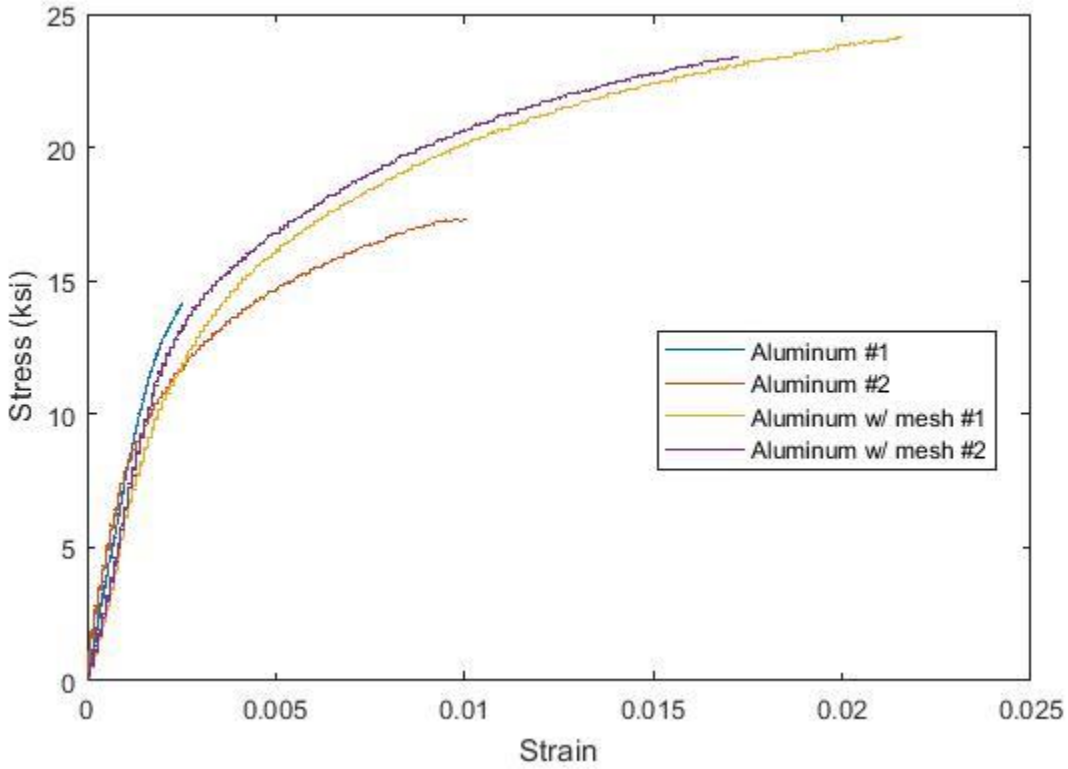

Figure 3.19: Tensile test data

Table 3.1: Summary of material properties

	Elastic Modulus(ksi)	Elongation at break	Ultimate Strength(ksi)
Al 356	7700	.60%	15.7
Al 356 with mesh	6800	1.9%	23.8
Al 356 reference [9]	10,500	>2.0%	19.0

An important observation was that in several instances, where tungsten mesh infiltration was poor, failure occurred by delamination of the layers of aluminum, instead of the whole specimen in tension. This occurred at values significantly lower than what is shown in Table 3.1. Poor mesh infiltration was immediately obvious after casting on several occasions. Inspection with SEM on a cut and polished surface, as shown in Figure 3.20, confirms this initial observation. When infiltration is poor, the aluminum on each side of the mesh is completely disconnected from the

other side. This makes the part two separate pieces of metal, instead of one solid piece. Poor infiltration can be avoided by using the larger mesh sizes. Other methods of improving infiltration could be implemented in future studies, since it appears critical to maintain favorable material properties. One such method could be coating the mesh with something to improve to wettability to liquid aluminum. Another possible method could be a forging or pressurized casting step to better force liquid aluminum into the gaps.

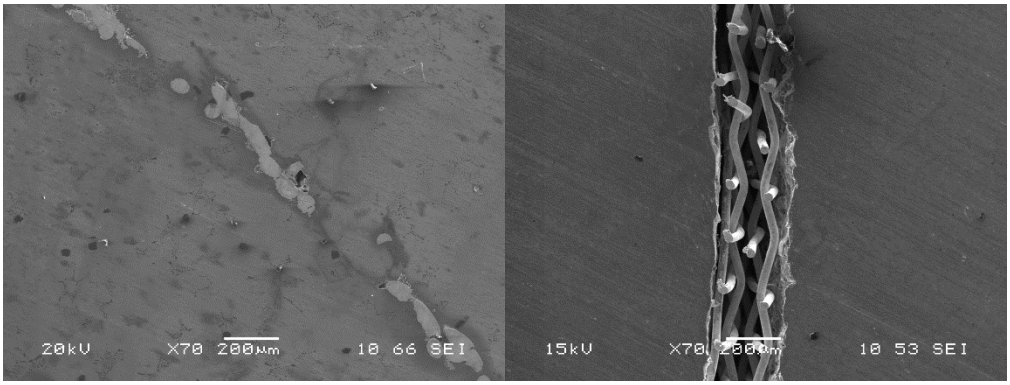

Figure 3.20: (L) SEM image of good mesh infiltration, (R) SEM image of poor mesh infiltration

CHAPTER 4: CONCLUSIONS AND RECOMMENDATIONS

4.1 Summary and Conclusions

Twenty nine tests were conducted to investigate the optimization of enhancements to an aluminum-based structural energetic case material. The enhancements previously identified to provide the best blast improvements were the alloying addition of magnesium and the inclusion of tungsten mesh within cast casings [3]. Baseline tests were performed to which performance could be compared. The parameters varied were the magnesium fraction added, the size of the tungsten mesh, and the number of wraps of tungsten mesh. Wall material was also varied to highlight the contribution of impact induced reaction of high speed fragments at the chamber walls. Additionally, material testing specimens were fabricated and tested to verify that aluminum enhanced with tungsten is still a structural engineering material. Finally, a combination case was made to combine the effects of magnesium and mesh.

By comparing the energy release to an unconfined bare charge, it was found that a low carbon steel case consumes 43% of the detonation energy in fracturing the steel and accelerating the subsequent fragments. Peak blast pressure and blast impulse were found to be decreased by similar amounts. A casing of the same mass, but made of unoptimized Al 6061, was found to have slightly less diminished blast characteristics as well as a much higher overall energy output, largely due to high speed aluminum fragments reacting upon impact with the steel chamber walls. It is calculated that for this baseline case 13% of the aluminum casing material must be reacting to release the observed energy. This corresponds to a 4.2 kJ/g specific energy on a casing mass basis.

The addition of magnesium as an alloying element in cast aluminum casings was found to improve all metrics by significant amounts. This is attributed to magnesium lowering the ignition temperature of the case material. The best performing alloy was found to be 20% magnesium. For this alloy, peak blast pressure and impulse were improved relative to the baseline case by 53% and 48%, respectively. QSP was found to be improved by 99% representing 12.2 kJ/g case specific energy and 40.3% case combustion. While much of this combustion occurs at the walls of the chamber, some must be occurring early in order to improve the blast and impulse metrics.

The variations in tungsten mesh size were less conclusive due to inconsistencies associated with the casting process involving tungsten mesh. In general, the data show that two wraps of any size

mesh embedded in a cast aluminum case can enhance the three measured metrics. QSP improvements of 50% to 80%, peak blast pressure improvements of 17% to 48%, and impulse improvements of 6% to 50% were observed. A larger sample size and more consistent manufacturing process might provide a more definitive answer in the future.

Variation of the number of wraps of tungsten mesh led to improvements in QSP ranging from 50% to 60%, improvements in peak pressure ranging from 10% to 35%, and improvements in impulse ranging from 10% to 28%. Similar to the mesh size variation, there is no obvious optimum number of wraps of mesh but all cases show significant improvements over baseline.

A top performing case was made using all previous data. A case was made using a 20% magnesium alloy with the slightly variation in manufacturing of adding the magnesium at the end of the casting process to reduce oxidation. Additionally, three wraps of size 18 tungsten mesh were embedded at separate locations. The result was the top performing case of the study. A 123% improvement in QSP, a 105% improvement in peak blast pressure, and a 102% improvement in impulse were observed compared to a baseline case. The improvements recover peak blast and impulse measurements above that of a bare charge. An energy calculation yields a case specific energy release of 14.2 kJ/g corresponding to 47% combustion of the case mass.

Standard tensile tests on specimens of aluminum with embedded tungsten mesh reveal that the inclusion of tungsten mesh at the very least does not weaken aluminum and may slightly improve strength. One caveat to this is that tungsten mesh infiltration must be relatively complete, otherwise failure occurs by delamination of materials at a much lower stress levels than plain aluminum. The method used in this study to improve mesh infiltration for the purposes of material testing was to use a larger size mesh as it was previously shown that blast performance does not significantly vary with mesh size.

4.2 Recommendations for Future Work

For future research, scaling of reactive case systems should be considered. Changing length scales as well as timescales could significantly affect the degree to which casing modifications enhance reactivity. Some degree of scaling could be performing in the same test chamber as this study.

There is now a larger (approximately 10x the volume) test chamber in the research group that could be used. Further scaling would likely require outdoor field testing.

Future testing should also improve upon the manufacturing process of cast composite casings. Methods of improving infiltration consistency should be investigated. These include but are not limited to coating the mesh with a metal more amenable to aluminum wetting, a forging step, and casting in an inert environment. This study has revealed that consistency in manufacturing of reactive cases is crucial to consistent blast characteristics.

Further material testing on structural reactive materials could also be performed. A larger sample size of tensile test specimens would be beneficial for characterizing strength of tungsten mesh-aluminum composites. The material properties of the top performing 20% Mg/ 80% Al alloy could also be characterized. Furthermore, compression testing and hardness testing could be performed. Typically compression characteristics are similar to tension but composites are a common group of materials where properties are not isotropic.

Lastly, a more detailed investigation of impact induced reaction could be performed. Impact induced reaction (IIR) was found to be a significant fraction of overall energy release for baseline cases but was not quantified for the enhancements tested in this study. Additionally, different wall materials such as steel, concrete, wood, and drywall could be characterized in some way to predict energy release by IIR from a reactive case system in a target structure. Amount of reactive material fragment combustion could also be investigated as a function of fragment velocity.

REFERENCES

[1] T. Ngo, P. Mendis, A. Gupta and J. Ramsay, “Blast Loading and Blast Effects on Structures – An Overview”, *Electronic Journal of Structural Engineering*, pp. 76-91, 2007.

[2] W. Baker, C. Anderson, B. Morris, and D. Wauters, “Quasi-static pressure, duration, and impulse for explosions in structures," *Minutes of the Twentieth Explosives Safety Seminar*, pp. 389-413, 1982.

[3] M. Clemenson, “Enhancing Reactivity in Aluminum-Based Structural Energetic Materials.” Ph.D. Thesis. University of Illinois at Urbana-Champaign. Dept. of Mechanical Engineering, 2015.

[4] E. Popov, L. Kashporov, V. Mal'tsev, and A. Breiter, “Combustion mechanism of aluminum-magnesium alloy particles," *Combustion*, Explosion, and Shock Waves, vol. 9, no. 2, pp. 204-208, 1973.

[5] P. Cooper, Explosives Engineering. Wiley-VCH, Inc., 1996.

[6] PCB Piezotronics, “Model 137B23B ICP Pressure Sensor Installation and Operating Manual.” Technical Manual. PCB Piezotronics. 2011.

[7] C. H. Chan, “Ignition Limits of Explosively Dispersed Fuel.” M.S. Thesis. University of Illinois at Urbana-Champaign. Dept. of Mechanical Engineering, 2015.

[8] J. Hilsenrath, “Tables of thermal properties of gases”, *NBS Circular* 564, 1955.

[9] Matweb.com. (2018). Aluminum A356.0-T6, Sand Cast. [online] Available at: http://www.matweb.com/search/datasheet.aspx?matguid=d524d6bf305c4ce99414cabd1c7ed070 [Accessed 5 Apr. 2018].

APPENDIX A – Example Pressure Calibration

Table A.1: Example static calibration of Kulite and Gems pressure transducers

Date	3/15/2018			
Pressure(psi)	**Lolly 2(V)**	**Lolly 4(V)**	**1304 GEMS(V)**	**1308 GEMS(V)**
-0.06	-0.0115	-0.00496	0.7987	0.8019
1.01	0.07098	0.163	0.8276	0.8302
2.04	0.1477	0.319	0.8544	0.8574
3.05	0.2265	0.4777	0.881	0.8843
4.02	0.301	0.6292	0.9071	0.9101
5.08	0.3845	0.7991	0.936	0.9393
4.53	0.3403	0.7094	0.9206	0.9239
3.55	0.2656	0.5576	0.8946	0.8978
2.56	0.1874	0.4002	0.8678	0.8712
1.58	0.1131	0.2486	0.8421	0.8453
0.54	0.03432	0.0888	0.8151	0.8182
Slope(psi/V)	13.00652	6.41144	37.62785	37.55676
Y-int(psi)	0.10072	-0.02101	-30.11435	-30.17079
r^2	0.99994	0.99995	0.99993	0.99995

APPENDIX B – Drawings of Machined Parts

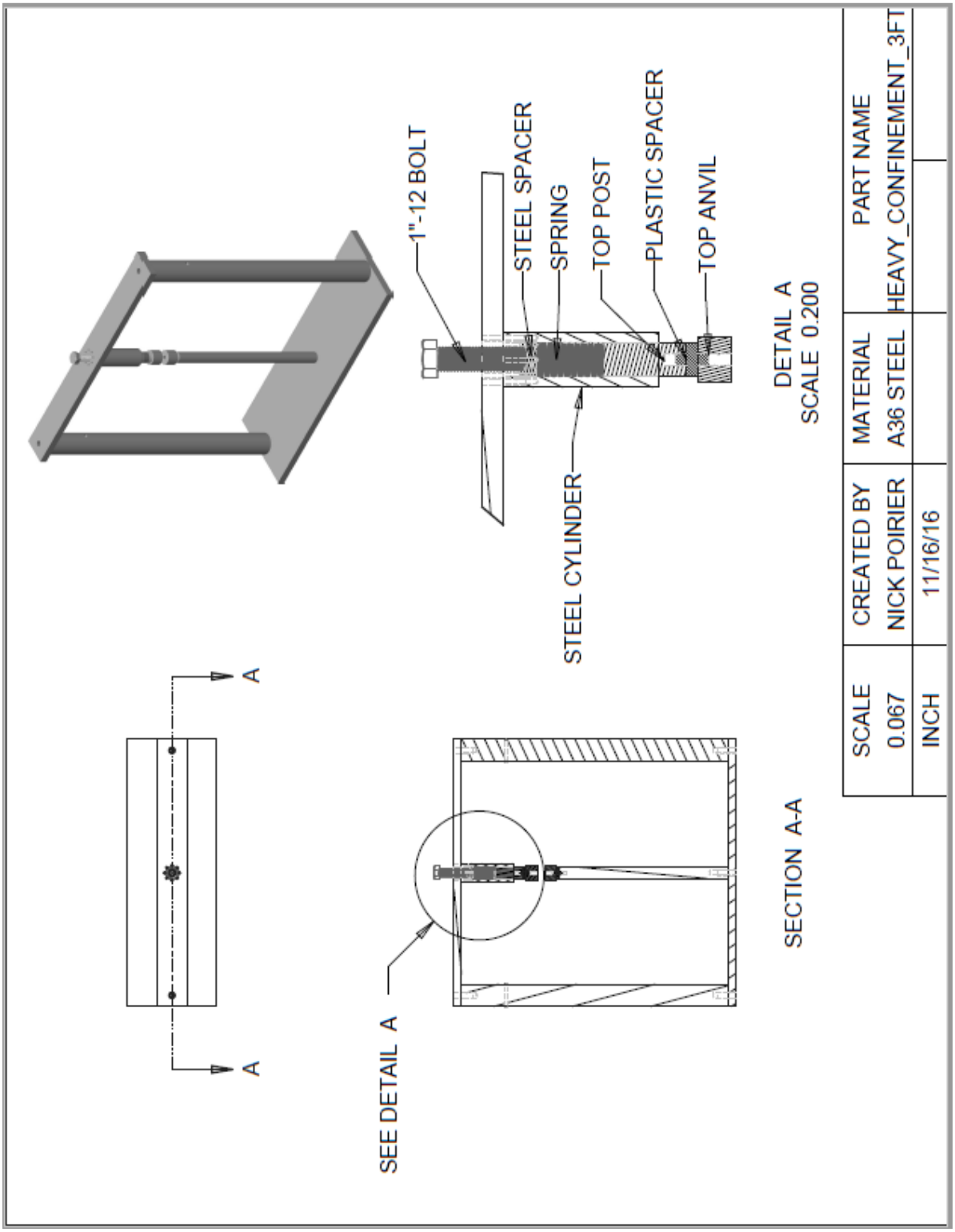

Figure B.1: Heavy Confinement Assembly view

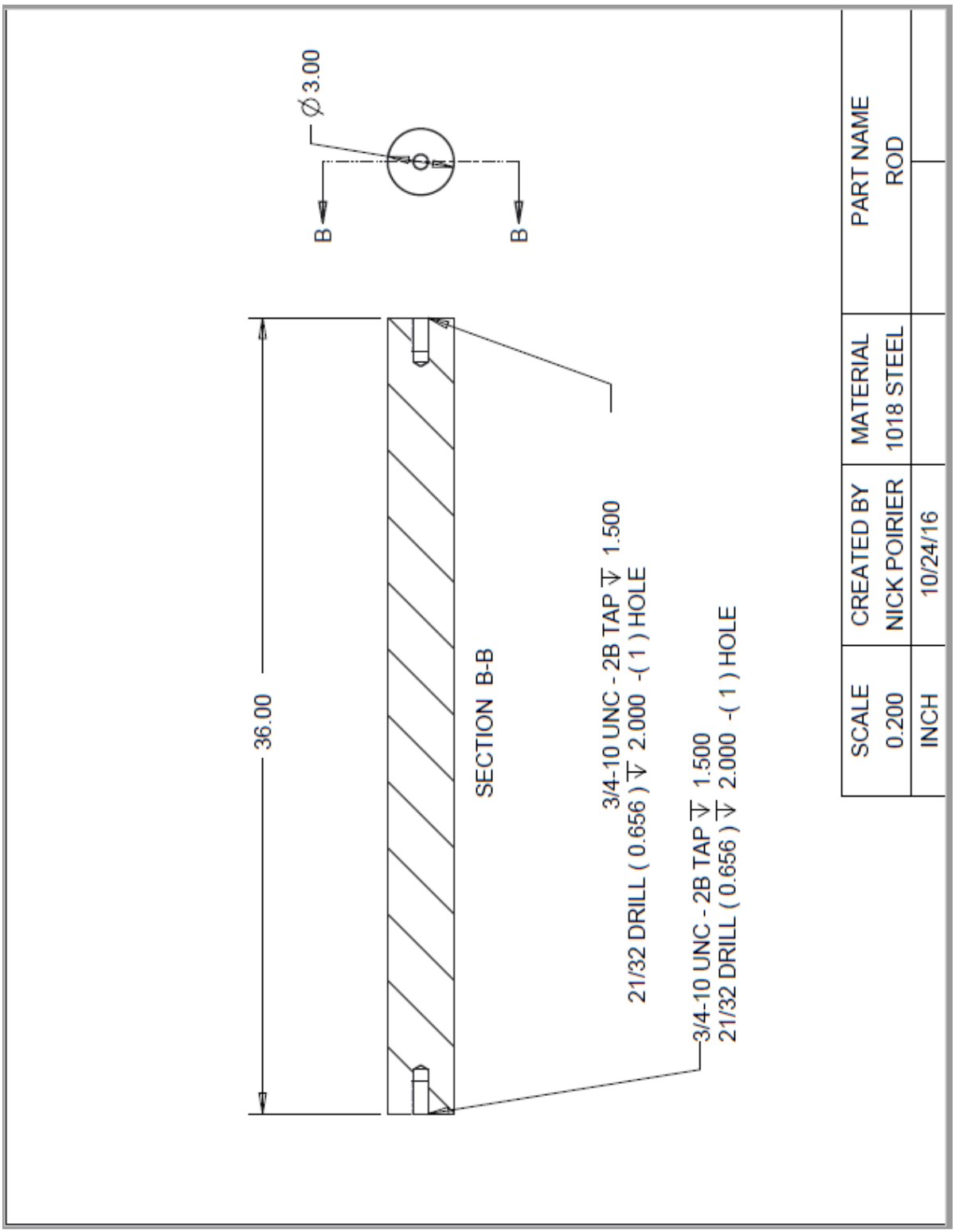

Figure B.2: Heavy Confinement Side Posts

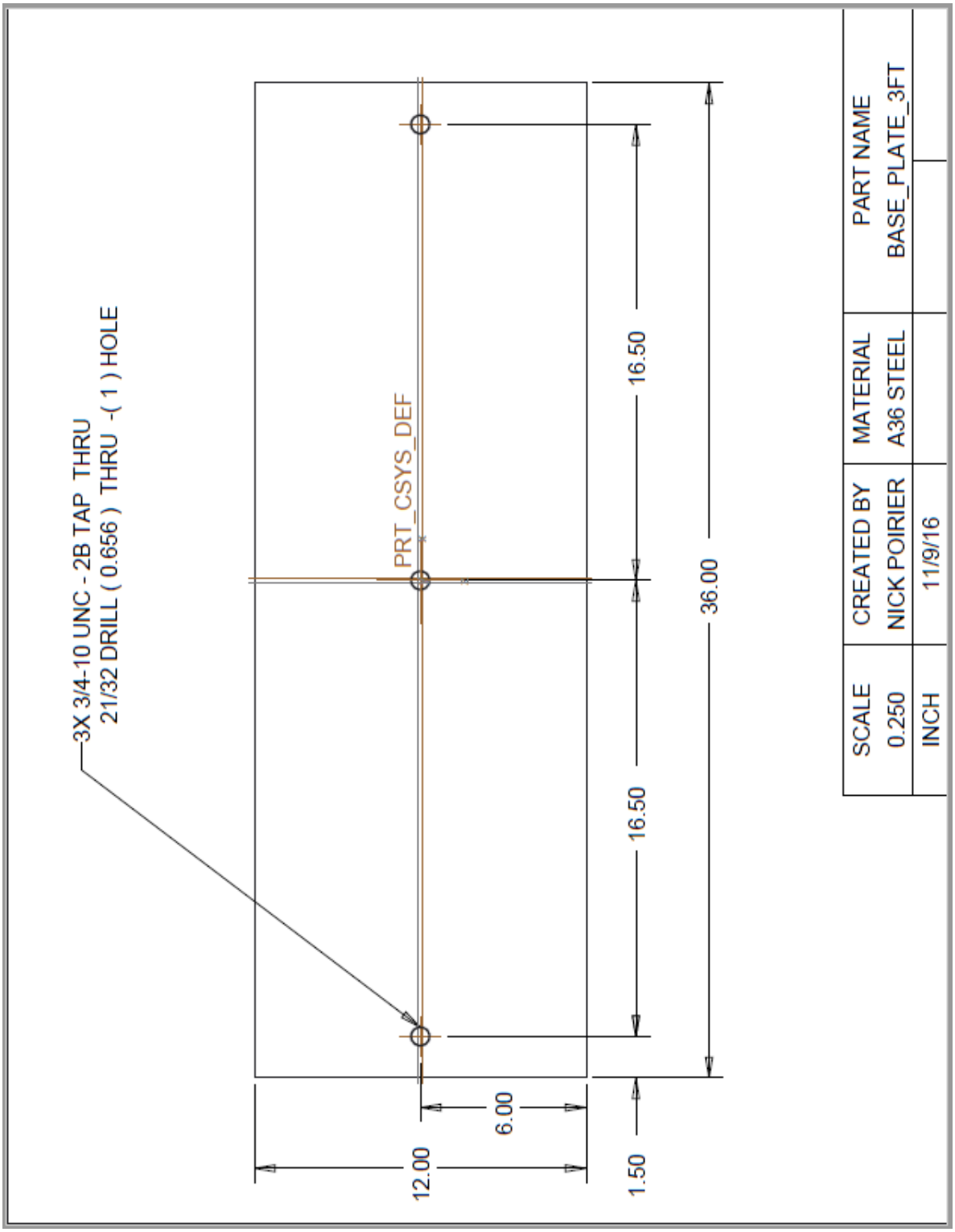

Figure B.3: Heavy Confinement Bottom Plate

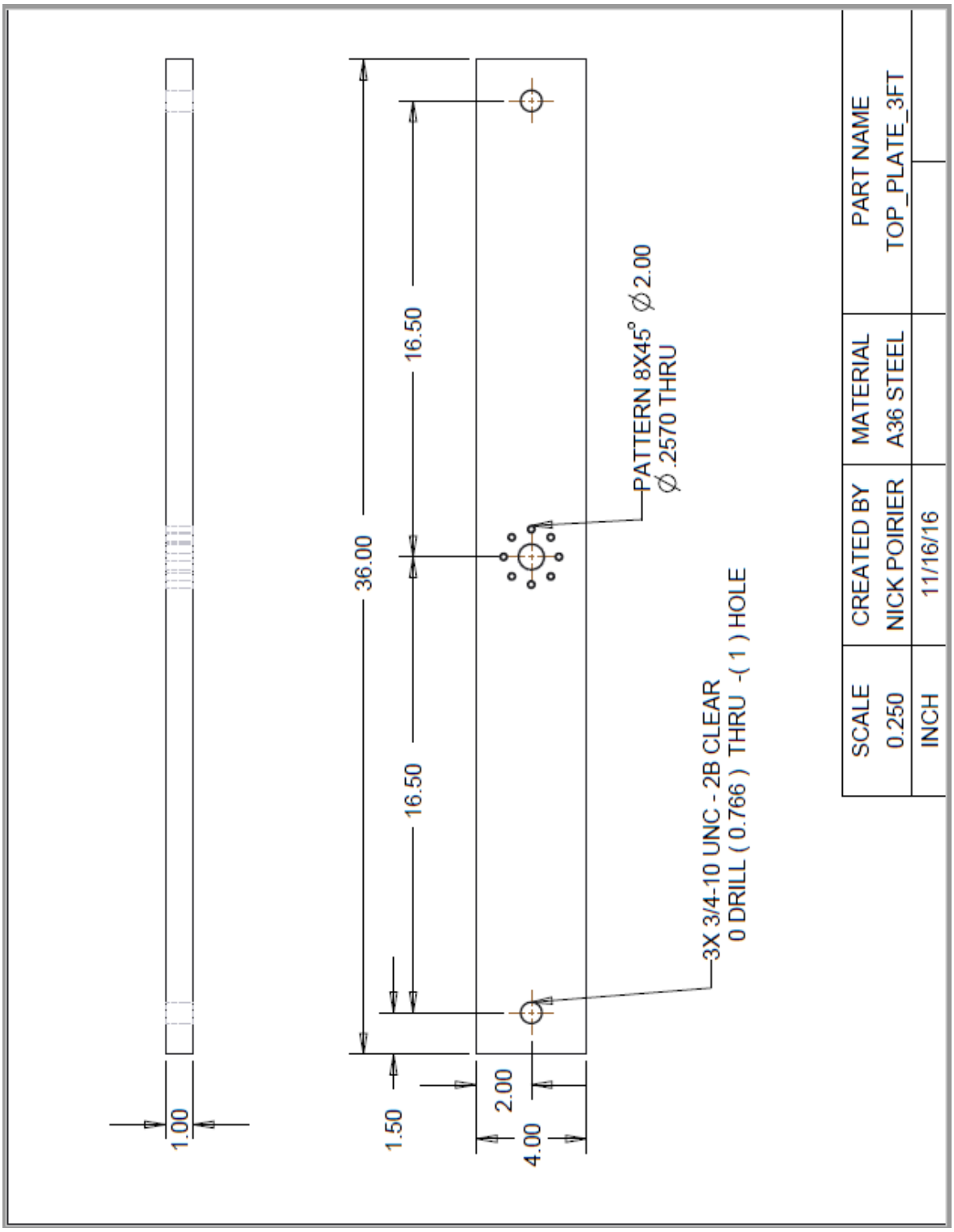

Figure B.4: Heavy Confinement Top Plate

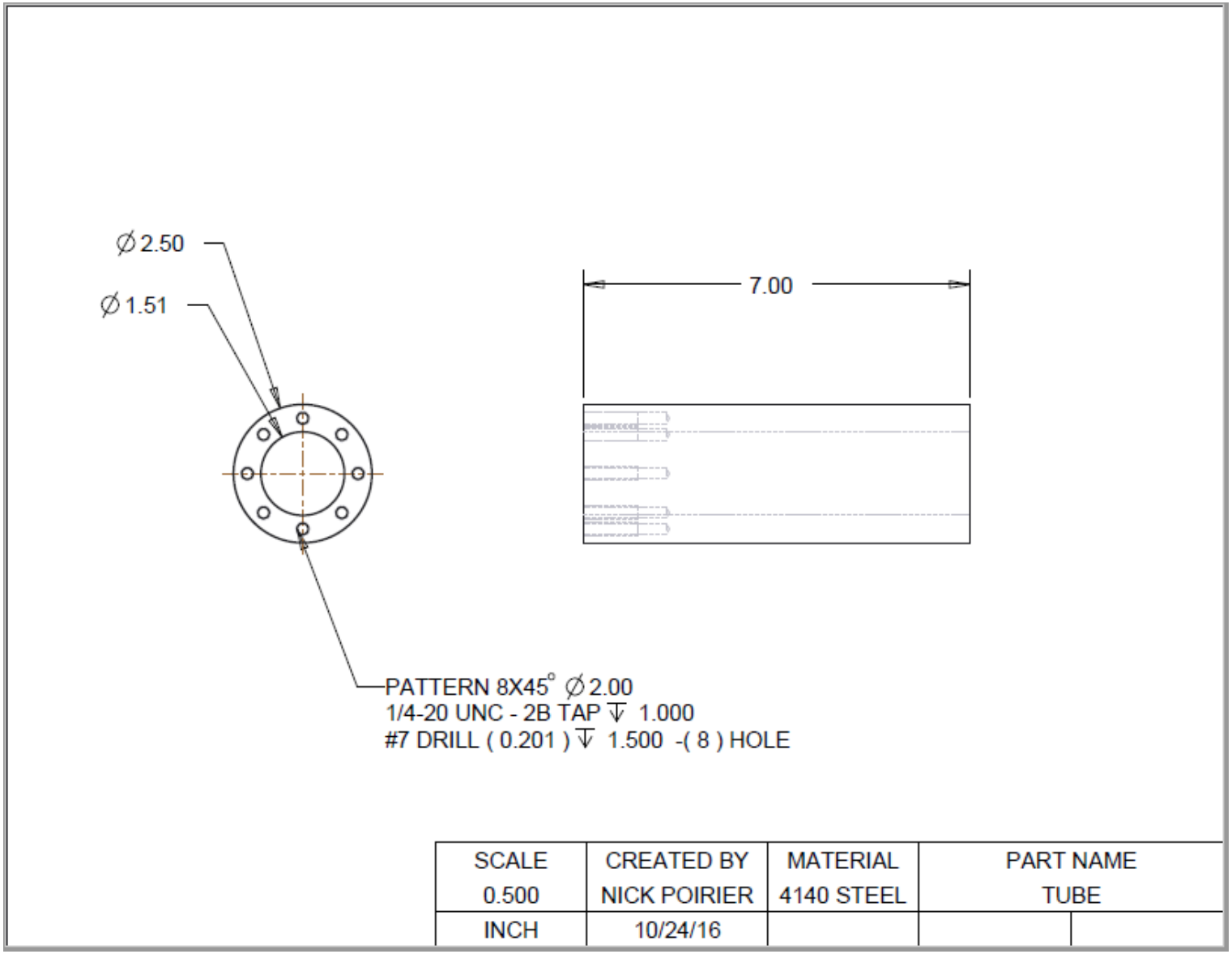

Figure B.5: Heavy Confinement Spring Tube

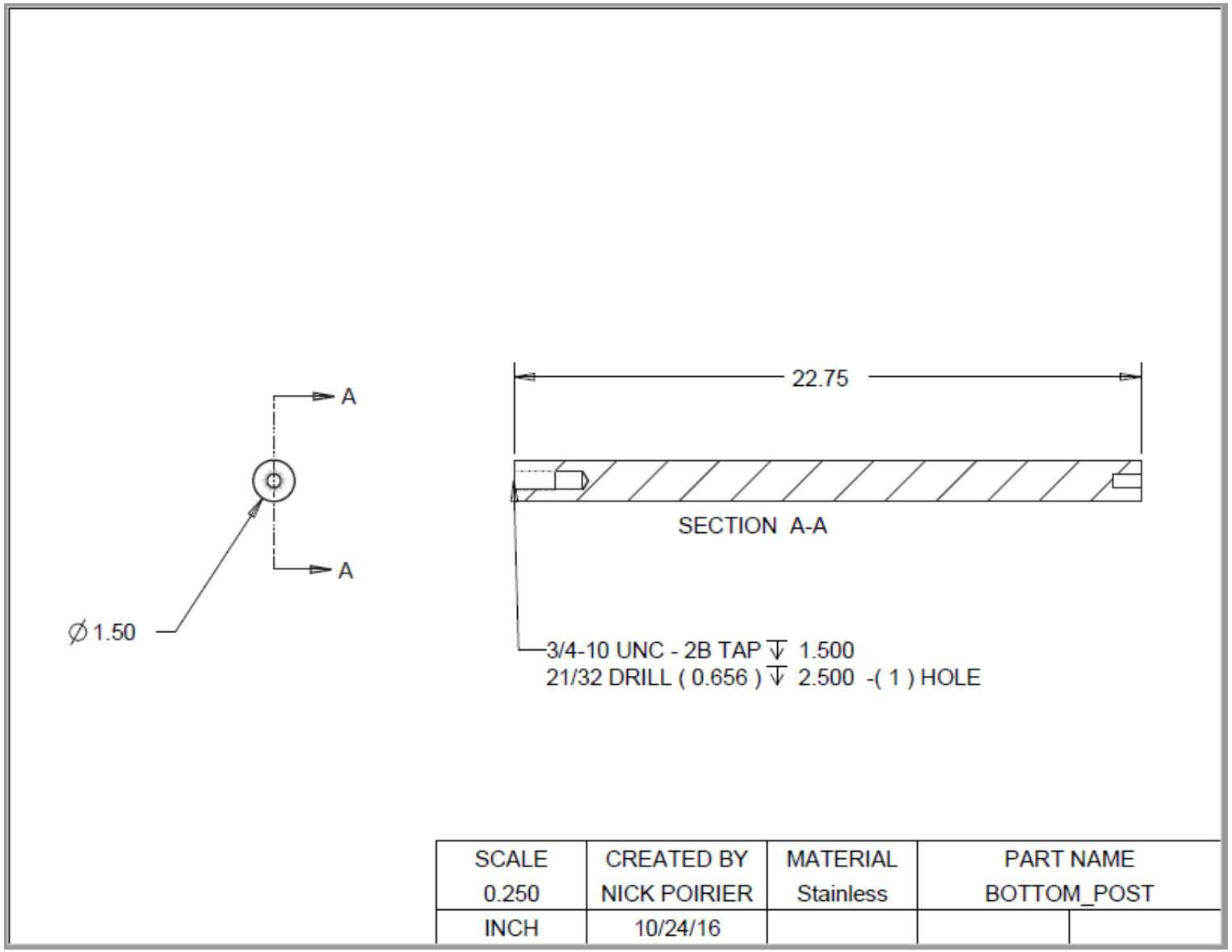

Figure B.6: Heavy Confinement Bottom Charge Post

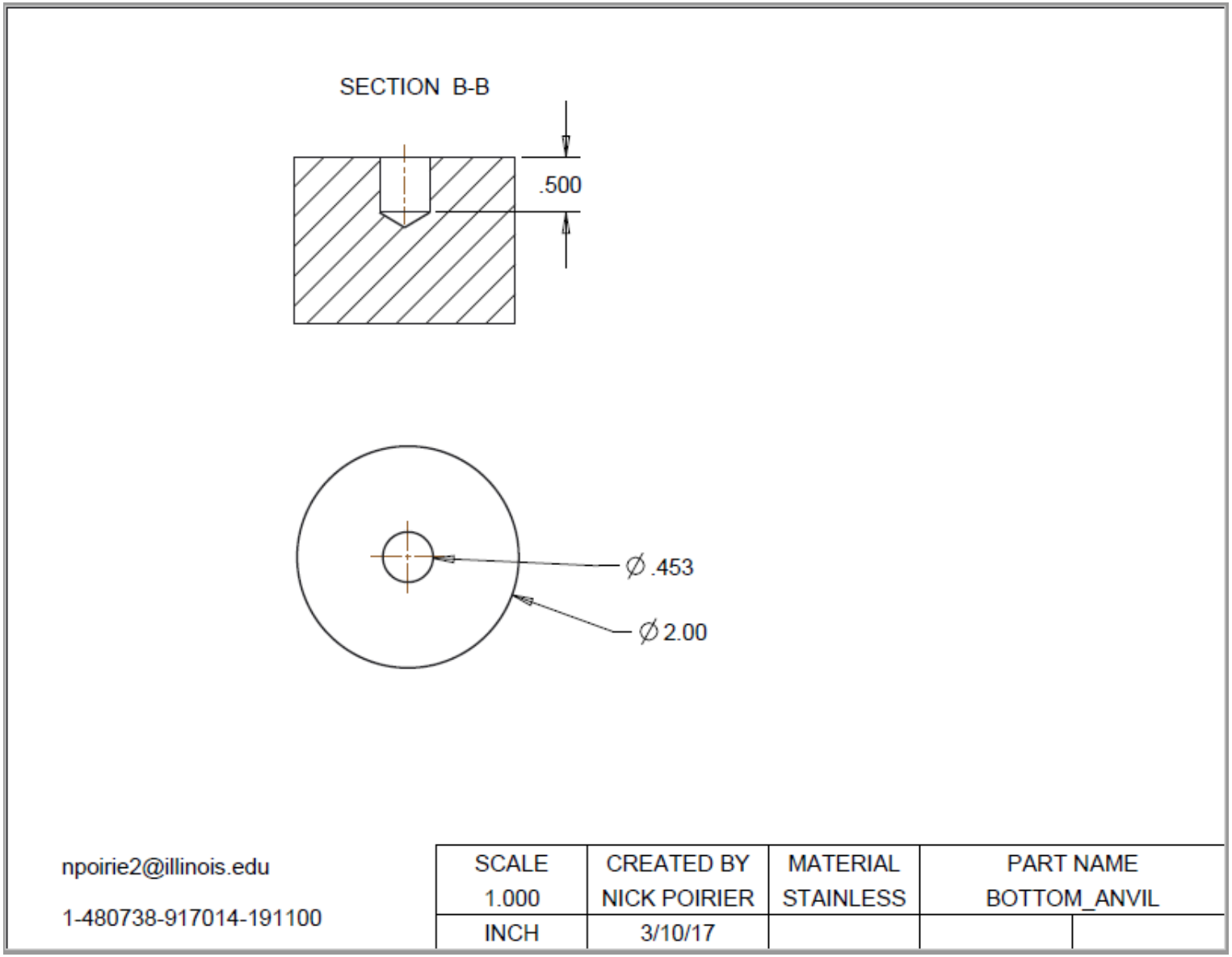

Figure B.7: Heavy Confinement Top Anvil

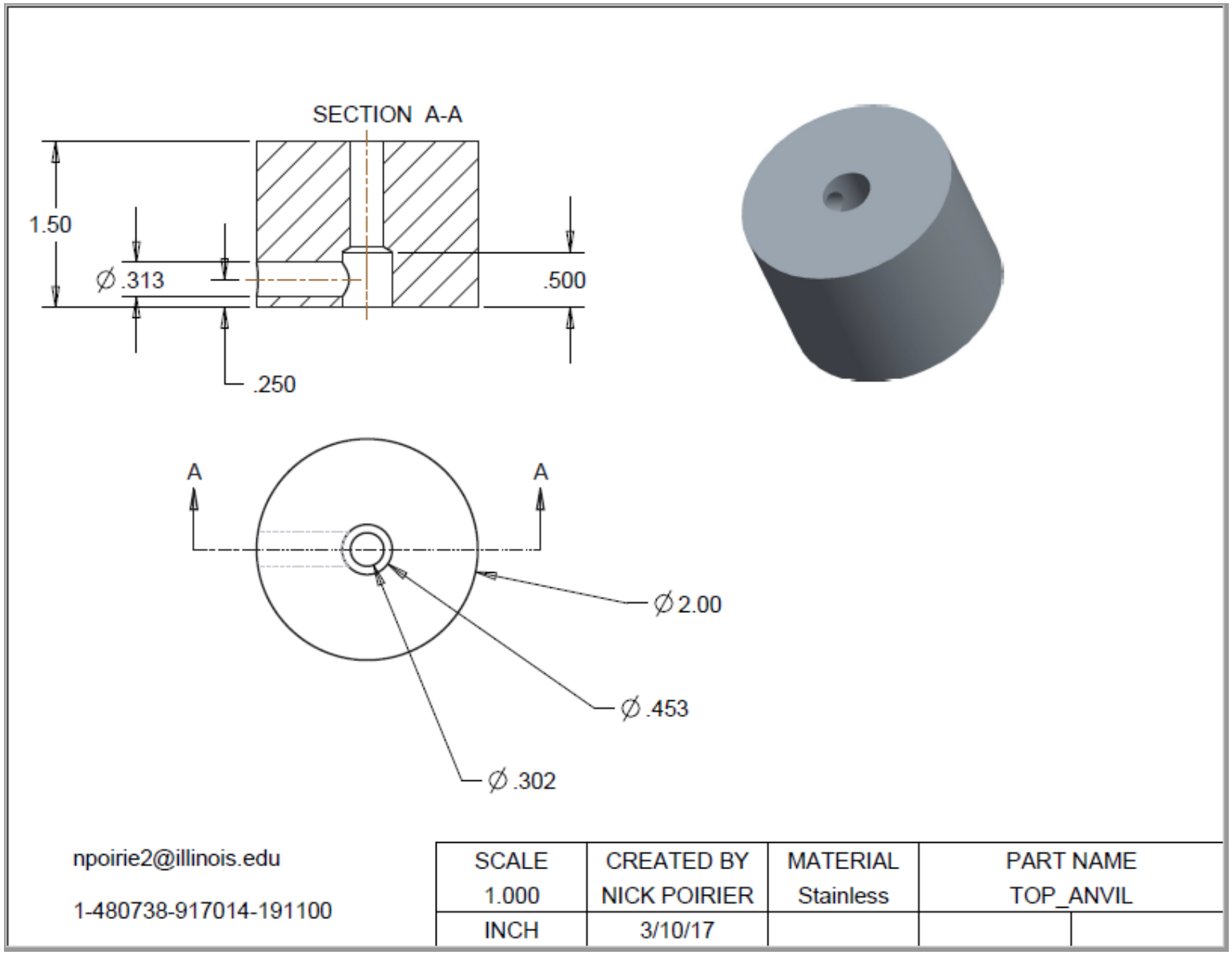

Figure B.8: Heavy Confinement Bottom Anvil

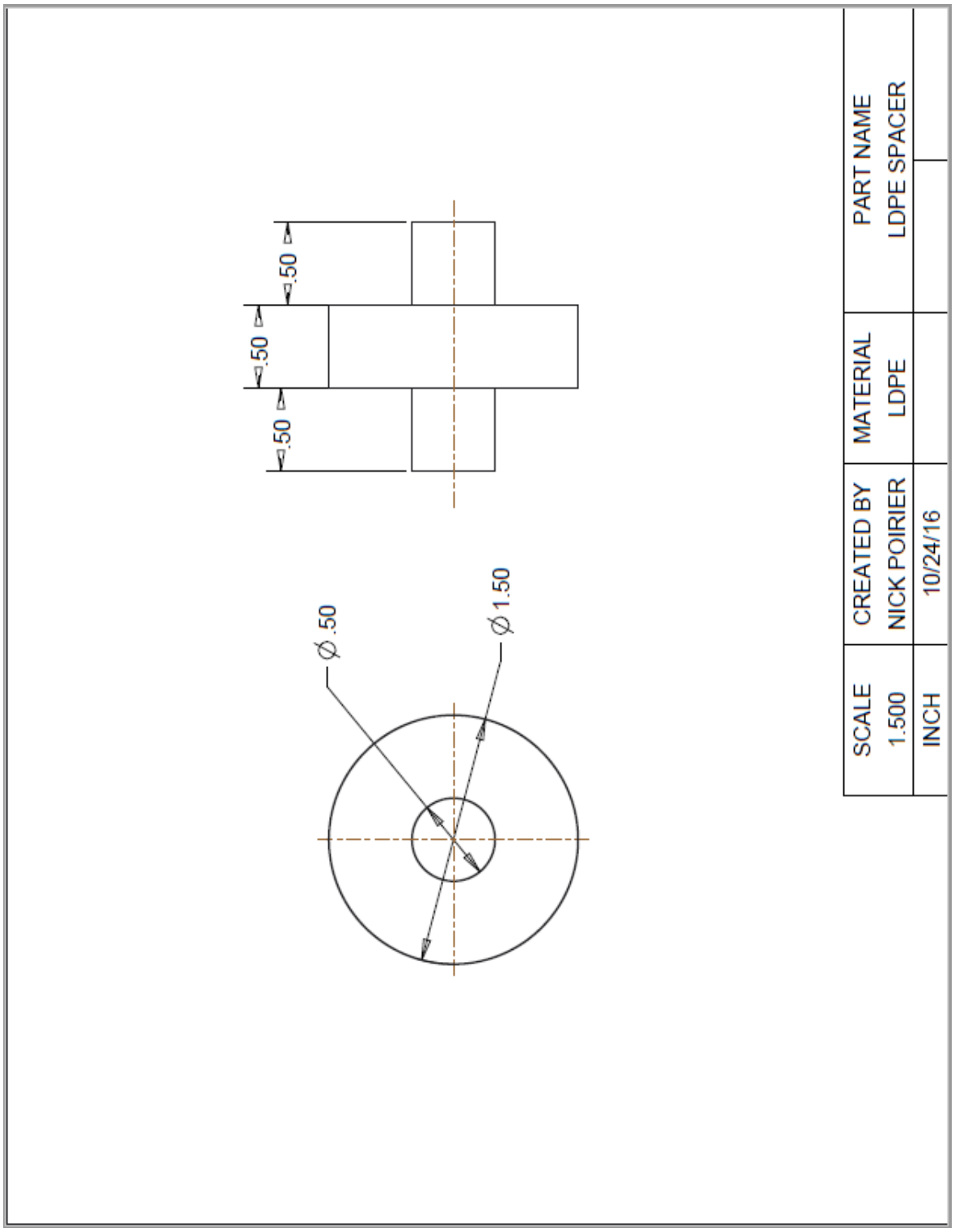

Figure B.9: Heavy Confinement LDPE Spacer

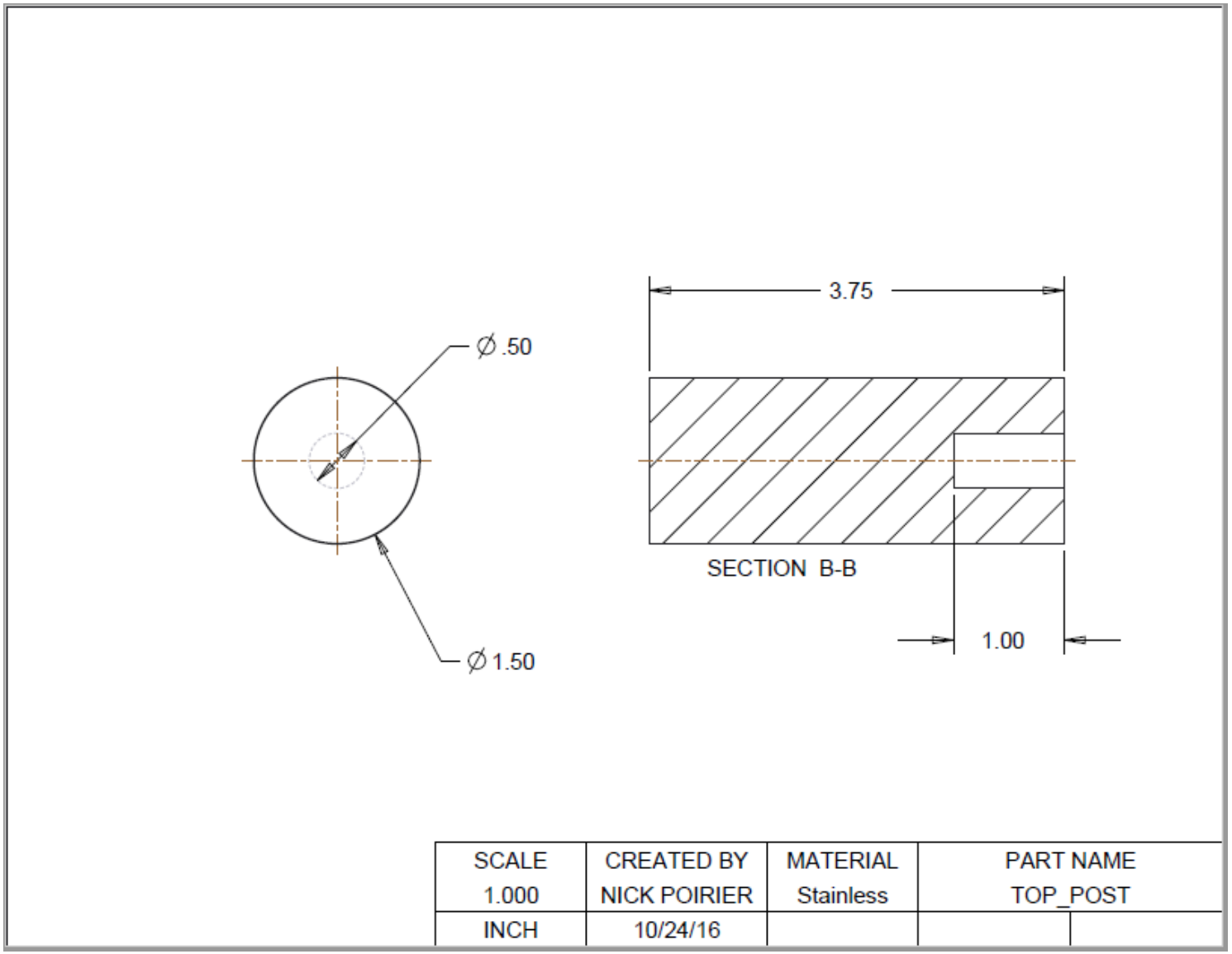

Figure B.10: Heavy Confinement Top Charge Post

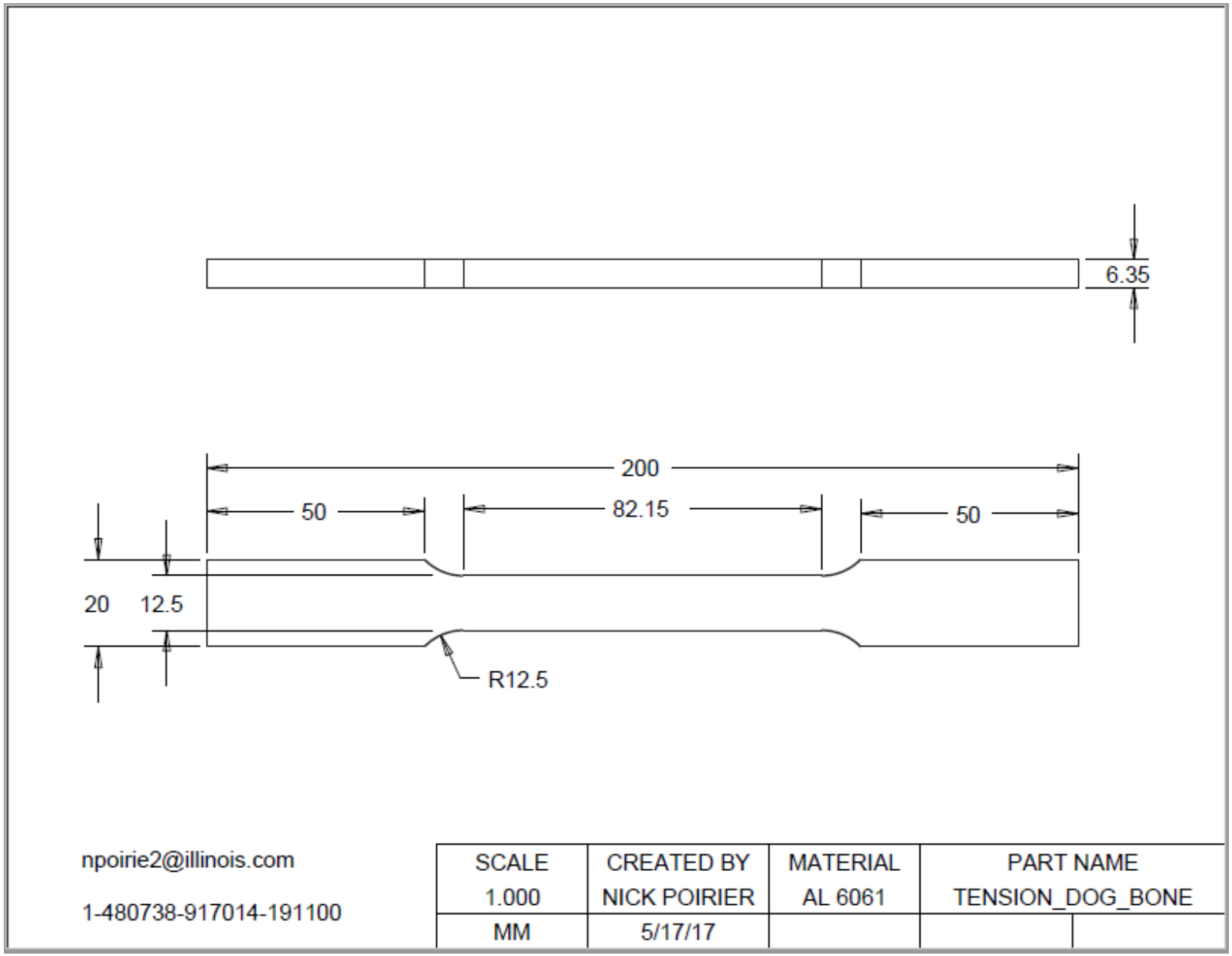

Figure B.11: Tensile test specimen

APPENDIX C – Complete Test List

Table C.1: List of all cases tested

Case #	Height(in)	ID(in)	OD(in)	Weight(g)	Mesh Size	Mg %	Wraps of Mesh	Notes
1	0.940	1.010	1.533	39.970	30	0%	2	
2	0.931	1.012	1.530	40.276	30	0%	2	Duplicate of #1
3	0.917	1.010	1.549	39.926	18	0%	2	Mesh is possibly shifted(non concentric)
4	0.929	1.023	1.534	40.012	50	0%	2	
5	0.925	1.021	1.535	40.064	50	0%	2	Duplicate of #4
6	0.951	1.007	1.502	39.975	None	10%	None	
7	0.939	1.016	1.520	39.995	30	0%	1	
8	0.930	1.015	1.514	39.770	None	10%	None	Duplicate of #6
9	0.945	1.012	1.546	39.450	100	0%	2	
10	0.916	1.010	1.545	40.157	100	0%	2	Duplicate of #9. Better infiltration than #9
11	0.891	1.006	1.540	39.914	None	15%	None	
12	0.907	1.009	1.525	40.229	None	5%	None	
13	0.916	1.016	1.528	40.160	None	5%	None	Duplicate of #12
14	0.917	1.009	1.530	40.149	30	0%	3	
15	0.915	1.008	1.543	40.196	30	0%	3	Duplicate of #14
16	0.922	1.011	1.554	40.260	None	20%	None	
17	0.916	1.013	1.569	40.06	None	20%	None	Duplicate of #16
18	0.902	1.007	1.535	40.02	None	15%	None	Duplicate of #11
19	0.912	1.010	1.555	39.997	None	25%	None	
20	0.919	1.011	1.554	40.16	None	25%	None	Duplicate of #19
21	0.926	1.013	1.521	40.11	18	0%	2	Duplicate of #3. Better infiltration than #3
22	0.936	1.010	1.500	40.01	None	0%	None	Al 6061 Baseline case
23	0.925	1.012	1.500	39.9	None	0%	None	Al 6061 Baseline case
24	0.932	1.009	1.497	40.12	None	0%	None	IIR baseline. 2 layers of 3/8" black rubber mats.
25	0.931	1.017	1.496	39.56	None	0%	None	IIR Baseline. 1 sheet of 7/16" OSB. Al 6061 20.01g N9
26	0.928	1.017	1.496	39.43	None	0%	None	IIR Baseline. 2 sheets o 7/16" OSB. Al 6061 20.01g N9
27	0.919	1.011	1.573	39.93	None	20%	None	20% Mg added and the end of casting instead of the beginning. 20.01g N5
28	0.93	1.015	1.581	39.3	18	20%	3	Al 6061. 3 wraps of mesh at different radial locations. Mesh was visible and inner surface
29	.917	1.018	1.216	40.23	None	None	None	Low carbon steel baseline